# Southern Annular Mode Persistence and Westerly Jet: A Reassessment Using High-Resolution Global Models

Ting-Chen Chen<sup>1</sup>, Hugues Goosse<sup>1</sup>, <u>Cécile Davrinche<sup>1</sup></u>, <u>Stephy Libera<sup>1</sup></u>, <u>Christopher Roberts<sup>2</sup></u>, <u>Matthias Aengenheyster<sup>2</sup></u>, <u>Kristian Strommen<sup>3</sup>, <del>Christopher Roberts<sup>2</sup></del>, <u>Malcolm Roberts<sup>4</sup></u>, <u>Rohit Ghosh<sup>5</sup></u>, <u>Jin-Song von Storch<sup>6</sup>, <u>Stephy Libera<sup>4</sup></u></u></u>

<sup>1</sup>Earth and Life Institute, Université Catholique de Louvain, Ottignies-Louvain-la-Neuve, Belgium <sup>2</sup>European Centre for Medium Range Weather Forecasting (ECMWF), Reading, United Kingdom <sup>3</sup>Department of Atmospheric, Oceanic, and Planetary Physics, University of Oxford, Oxford, UK <sup>4</sup>Met Office Hadley Centre, Exeter, United Kingdom

O SAlfred Wegener Institute Helmholtz Centre for Polar and Marine Research, Bremerhaven, Germany Max-Planck Institute for Meteorology, Hamburg, Germany

Correspondence to: Stephy Libera (stephy.libera@uclouvain.be)

15

Abstract. This study evaluates the performance of high-resolution (grid sizes of 9–28 km for the atmosphere; 5–13 km for the ocean) global simulations from the EERIE project in representing the persistence of the Southern Annular Mode (SAM), a critical driver of Southern Hemisphere climate variability. Using the decorrelation timescale of the SAM index (τ), we compare EERIE coupled and atmosphere only (AMIP) simulations with CMIP6 and ERA5 datasets. EERIE coupled simulations improve the long-standing biases in SAM persistence, especially in early summer, with τ values of 9–17 days compared to CMIP6's 9–32 days. This improvement generally correlates with a more accurate climatological jet latitude (λ<sub>0</sub>) distribution in EERIE simulations than in CMIP6, but such a correlation is not robust within EERIE AMIP simulations with a well-represented jet location, suggesting other factors in play. With prescribed SSTs, EERIE AMIP show even smaller biases in both τ and λ<sub>0</sub> than EERIE coupled runs, highlighting the critical role of SST representation. Using the same AMIP model, finer grids (9 km vs. 28 km) can further reduce τ, but the underlying cause remains unclear, likely because of potential compensation between different processes. Sensitivity experiments filtering ocean mesoscale features in SST boundary conditions suggest that mesoscale processes enhance SAM persistence by ~2 days in early summer, though this effect is clear in ensemble means at 28 km but not in the single 9 km

runs. We also show that the atmospheric eddy feedback strength is a better indicator than  $\lambda_0$  to infer the SAM persistence, although the metric alone does not fully explain the  $\tau$  differences across SST scenarios. These findings underscore the interplay of dynamic processes influencing SAM persistence and offer insights for advancing global climate model performance. leading mode of Southern Hemisphere climate variability. Using the decorrelation timescale of the SAM index ( $\tau$ ), we compare EERIE simulations with CMIP6 models and ERA5 reanalysis.

EERIE simulations reduce long-standing biases in SAM persistence, especially in early summer, with  $\tau$  values of 9–20 days compared to CMIP6's 9–32 days and ERA5's 11 days. This improvement correlates with a more accurate climatological jet latitude ( $\lambda_0$ ). EERIE atmosphere-only AMIP runs outperform the coupled simulations in both  $\tau$  and  $\lambda_0$ , showing smaller biases and ranges of variability, underscoring the critical role of SST representation in shaping atmospheric circulation. In these AMIP experiments, the atmospheric eddy feedback strength, combined with the damping timescale estimated via friction, correlates more strongly with  $\tau$  than  $\lambda_0$ . We speculate that the well-captured jet position (biases <1° relative to ERA5), due to prescribed SSTs, limits  $\lambda_0$ 's explanatory power for  $\tau$  differences, allowing other processes to dominate. Using a finer model grid (9 km vs. 28 km) of the same AMIP model results in reduced  $\tau$ , though the mechanism remains unclear. Finally, motivated by the importance of oceanic eddies in the Southern Ocean, we conducted sensitivity experiments that filter transient mesoscale features from the SST boundary conditions. The results suggest that oceanic eddies may enhance summertime SAM persistence (by ~2 days), though this signal is not statistically significant and is absent in the single 9-km run, pointing to a subtle role of mesoscale ocean-atmosphere interaction that remains to be explored.

## 1 Introduction

35

40

45

Over the extratropical Southern Hemisphere, the daily- to decadal climate variability is dominated by the Southern Annular Mode (SAM), a mode of natural variability manifested in the large-scale oscillation of atmospheric mass between mid- and high-latitudes and hence the north-southward shift and intensity changechanges of the eddy-driven jet in the midlatitudes (e.g., Fogt and Marshall, 2020). This internal variability both influences and is influenced by the atmospheric circulation, affecting regional temperatures and precipitation patterns, sea ice extent, and ocean circulation, with consequences for

global heat and carbon redistribution (e.g., Doddridge and Marshall, 2017; Gillett et al., 2006; Lefebvre and Goosse, 2005; Lenton and Matear, 2007; Lovenduski and Gruber, 2005).

As inferred by its name "annular", the spatial structure of SAM is approximately "ring-shaped" when viewed from above the South Pole and is nearly barotropic in the vertical direction (Gerber et al., 2010).

During the positive phase of SAM, lower air pressure anomalies overlay Antarctica while higher pressure anomalies spread over the mid-latitudes, and such anomalous pressure distribution indicates a strengthening and poleward shifting of the westerly jet that climatologically sits at around 50°S (Lim et al., 2013). While the SAM can, to a first approximation, be described from a zonal-mean perspective, its structure can deviate from the zonal mean and vary across different timescales, affected by factors such as the seasonal cycle of midlatitude jet (atmospheric eddy activity), sea surface temperature (SST) variability, tropical oscillations such as the El Niño-Southern Oscillation (ENSO), stratosphere-troposphere interactions and so on (e.g., Campitelli et al., 2022; Ding et al., 2012; Fogt and Marshall, 2020; Karoly, 1989). On the seasonal scale, SAM is overall more zonally symmetric in austral summer (DJF) but exhibits asymmetric wavenumber 3 components when entering springautumn (MAM) and 0 summerwinter (JJA). Readers interested in a comprehensive review of the SAM literature are encouraged to consult Fogt and Marshall (2020) and Thompson et al. (2011).

An important A key characteristic of SAM is its temporal persistence, referring to how long a given phase of the SAM (positive, negative or neutral) tends to last before transitioning. If This long persistence is important as it provides a source of predictability at a timescale longer than the one associated with synoptic variability (e.g., Robinson 2000; Lorenz and Hartmann 2001, Simpson and Polvani 2016). SAM persistence is often measured as the decorrelation timescale (e-folding timescale) which indicates the average duration over which the SAM index remains strongly correlated with its past values. A standard explanation attributes the extended SAM persistence to the reinforcement of westerly flow anomalies by atmospheric eddy momentum fluxes, which are generated by changes in the mean flow and act to counteract dissipation from surface friction. Several mechanisms can be at the origin of this eddy-mean flow feedback that reinforces the shifted jet, including barotropic processes related to anomalous wave propagation and breaking and baroclinic processes associated with eddy generation and enhanced baroclinicity in the lower troposphere in response to shift in the westerly flow (e.g., Robinson 2000,

Lorenz and Hartmann 2001, Zurita-Gotor et al. 2014, Hassanzadeh and Kuang, 2019). The westerly flow anomalies also induce changes in the diabatic heating and cooling due to latent heat release and cloud radiative effect that modify the temperature gradients, affecting SAM persistence (Xia and Chang 2014, Smith et al. 2024, Vishny et al. 2024). In addition to this eddy-mean flow feedback, SAM persistence can have an origin from the stratosphere, which introduces some non-stationary forcing to SAM. The main influence is likely in late spring and summer at the time of the seasonal breakdown of the stratospheric vortex (Simpson et al. 2011, Byrne et al. 2016, Byrne et al. 2017, Saggioro and Shepherd 2019). Furthermore, interactions between a stationary mode and a propagating mode of the zonal variability could also affect SAM persistence (Lubis and Hassanzadeh 2021, Sheshadri and Plumb 2017, Smith et al. 2024).

While global climate models (GCMs) have shown good skills in capturing the spatial structure of SAM variability, a long-standing eommon-challenge for GCMs is that they tend to overestimate the SAM persistence during the austral summer. Based on global reanalysis data, the SAM decorrelation timescale is found to be approximately 10 days on annual mean and is a couple of days higher in early summer (November–January; NDJ), during which period GCMs typically show values that are two to three-times larger (Bracegirdle et al., 2020). Many studies have found a strong dependency between the SAM persistence bias and the bias in the climatological westerly jet location (e.g., Kidston and Gerber, 2010; Simpson et al., 20132013a, b; Simpson and Polvani, 2016; Son et al., 2010), that is, GCMs showing too persistent SAM tend to be associated with a too equatorward-placed tropospheric westerly jet. A possible explanation for such a relationship is that the structure of the climatological jet can affect the tropospheric eddy-mean flow feedback, the process by which small-scale atmospheric eddies interact with large-scale elimate anomalies to amplify them, and models with lower latitude jets exert stronger feedback to maintain SAM (Codron, 2005; Simpson and Polvani, 2016).

However, the climatological position of the midlatitude jet is not the only factor for the overly persistent SAM variability in GCMs. Simpson et al. (2013a) performed a series of experiments with nudging and bias correcting procedures using a stratosphere-resolving GCM, the Canadian Middle Atmosphere Model (CMAM). They found that the SAM persistence bias remains even when the representation of the climatological tropospheric winds is artificially improved. Similar conclusions are obtained when another

common bias for the overly-persistent summertime SAM —specifically, the delayed breakdown of the stratospheric vortex— was manually nudged toward the reanalysis-based seasonal climatology. Based on these results, they suggested that a substantial proportion of the SAM timescale bias arises from "internal" tropospheric dynamics, specifically the atmospheric eddy-mean flow feedback.

115

120

125

130

135

Such a feedback mechanism assumes that the shifted midlatitude jet associated with the positive/negative SAM acts as a source of eddies. When eddies propagate away from the source region before breaking, convergence of eddy vorticity flux is produced in the upper troposphere. Such eddy vorticity flux convergence can reinforce the shifted jet by enhancing the baroclinicity through adiabatic heating/cooling associated with the induced secondary circulation, thus extending the SAM persistence against dissipation from surface friction. Within this framework, Barnes and Hartmann (2010) performed a budget analysis of the relative vorticity tendency equation in a global reanalysis. Their analysis showed that this feedback is present across the hemisphere in austral summer but lacking over the western Pacific in winter due to a weaker climatological midlatitude jet in that region. Such a seasonal variation appears to explain the longer SAM timescale in summer than in winter. Following a similar concept, Simpson et al. (2013) performed momentum budget analysis of the vertically averaged and zonally averaged zonal wind associated with SAM and confirmed that the maintenance of SAM anomalous wind is dominated by the eddy momentum flux convergence that compensates the negative contribution by friction. They also showedSimpson et al. (2013b) examined the Coupled Model Intercomparison Project Phase 5 (CMIP5) climate models, and found that the overly persistent SAM is highly correlated (coefficient of 0.83) with the too strong total eddy feedback during the summer season in the Coupled Model Intercomparison Project Phase 5 (CMIP5) climate models..

As GCMs improve in their representation of physics, resolution, and overall complexity, some advancements have been made in reducing biases associated with SAM persistence and the climatological jet latitude. Compared to earlier versions of CMIP models (e.g., CMIP3, CMIP5), noticeable reductions in these biases have been reported. Bracegirdle et al. (2020) found that the ensemble-mean bias in the westerly jet latitude decreased from 1.9° in CMIP5 to 0.4° in CMIP6 on an annual mean basis. Consistently, the early-summertime SAM persistence was reduced from approximately 30 days in CMIP5 to 20 days in CMIP6. Nevertheless, the SAM decorrelation timescale remains systematically biased.

140 While higher resolution is generally regarded as beneficial, it is worth exploring whether additional improvements are achievable by further increasing the resolution or if other factors become increasingly significant when the resolution has reached beyond a sufficiently high level.

145

155

160

This potential role of an increase in resolution in reducing the biases in SAM persistence and the relationship with the mean-state westerly jet is investigated here in new experiments conducted as part of the Horizon Europe project European Eddy-Rich Earth System Models (EERIE) (M. J. Roberts et al., 2024a). A distinctive feature of the high resolution atmosphere-ocean coupled Earth System Models (ESMs) built under EERIE is their adoption of high oceanic resolutions to explicitly represent ocean mesoscale processes, which have been increasingly recognized as critical for weather and climate simulation in recent studies (e.g., Busecke and Abernathey, 2019; Chassignet and Xu, 2021; Hewitt et al., 2020). Mesoscale oceanic features can influence SAM persistence by strongly affecting surface heat fluxes and surface stress in the Southern Ocean—a hotspot of mesoscale activity (Frenger et al., 2013; Bishop et al., 2017). These ocean-atmosphere interactions can alter atmospheric temperature gradients and boundary layer structure, modifying diabatic heating and low-level baroclinicity, both of which have been linked to SAM persistence (Xia and Chang, 2014; Smith et al., 2024; Robinson, 2000; Zurita-Gotor et al., 2014). Furthermore, surface stress also plays a role as it tends to damp the westerly winds but also to enhance baroclinicity and the baroclinic feedback (Robinson 2000, Zurita-Gotor 2014, Vishny et al. 2024).

In addition to the development of new coupled models, EERIE also includes a suite of atmosphere-only simulations and idealized experiments to facilitate exploration of the atmosphere response to the ocean mesoscales by excluding effects attributed to the air-sea coupling and SST biases. Those experiments will allow disentangling the role of the explicit resolution of the eddies compared to the one of increasing the model resolution. Using those experiments, we specifically analyze the potential role of the mesoscale oceanic eddies on SAM persistence, a contribution that has been studied to a minimum to date. The data sources and diagnostics are detailed in Sections 2 and 3, respectively, followed by the results in Section 4 and the conclusions in Section 5.

#### 2 Data

170

175

180

185

190

#### 2.1 EERIE models & simulations

Running from January 2023 to December 2026, the EERIE project aims to build new generations of ESMs run at "eddy-rich resolution" (note that the "eddy" here refers to ocean eddies), which explicitly resolve ocean mesoscale processes with scales of 10–100 km. Crucial components at this scale include the ocean eddies (analogous to cyclones in the atmosphere) and boundary/frontal currents. EERIE will deliver simulations over multi-centennial timescales centered on four global coupled ESMs and two atmosphere-only models, with an overarching objective to reveal and to quantify the role of ocean mesoscales in shaping the climate trajectory over seasonal to centennial time scales, regionally and globally (European Commission, 2022). The simulations are organized in two phases, with the Phase 1 providing guidance for the planning of Phase 2.

# 2.1.1 Coupled simulations

This study evaluates the preliminary EERIE Phase 1 simulations based on their (Wachsmann et al., 2024). To facilitate direct comparison across experiments, all outputs were regridded output onto a uniform 0.25° ×0.25° grid (Wachsmann et al., 2024). prior to analysis, except for the westerly jet location identification (Section 3.2). A detailed description of the EERIE models can be found in M. J. Roberts et al., (2024a), and here weTable 1 briefly summarizes the simulations used in the current study (Table 1). We analyze five coupled. IFS-FESOM2 and ICON model simulations in total: fourare conducted following a protocol similar to the CMIP6 HighResMIP (High Resolution Model Intercomparison Project; Haarsma et al., 2016), using either the IFS-FESOM2 or ICON models, and one following similar). The HadGEM3-GC5-EERIE model simulation follows protocol similar as CMIP6 DECK (Diagnostic, Evaluation and Characterization of Klima; Eyring et al., 2016) with the HadGEM3-GC5-EERIE model.). HighResMIP differs from CMIP6 DECK primarily in its use of 1950s' climate conditions instead of 1850s' as the initial state and a shorter spin-up (~50 years instead of >= 200 years; which have been discarded and not counted in the simulation length shown in Table 1) due to the computational demands of high-resolution models. Using the IFS-FESOM2 model, we analyze selected segments of the spin-up and a 65-year control runs (referred to as 1950spinup and 1950centrol), both simulation

conducted under fixed 1950 forcings. The analyzed segments vary in length depending on data availability, as detailed in Table 1. Additionally, we examine a portion of the (referred to as 1950control), along with a historical simulation covering the period from 1950–1969. to 2014. For the ICON model, only—the 22-year 1950control and the 1950spinuphistorical run is available are analyzed. For the HadGEM3 model, we investigate the examine a 30-year pre-industrial control simulation (piControl) forced by 1850 conditions.

While As these simulations cover different time periods, we do not expect these differences to significantly impact the evaluation of specific model performance in SAM persistence, as—and some of them include transient forcing, linear and low-frequency nonlinear trends and a slowly varying climatology—are removed as standard procedures in the SAM-related diagnostics. However, it This should be borne in mind that-reduce the impact of the difference in experimental design on the evaluation of the model performance. However, this removal maydoes not fully eliminate all the non-stationary features in the second moments. Therefore, when evaluating EERIE runs against that could have a clear influence on the evaluation of SAM persistence and of the eddy feedbacks (Byrne et al. 2016). We therefore adopt a bootstrapping procedure (Section 3.1) to provide partial quantification of the influence of non-stationarity and uncertainty due to the short period of some simulations. As will be shown later, through bootstrapping resampling, different results can be obtained with the same model even after de-trending. We also provide results using two different periods of the ERA5 reanalysis (Section 2.2), a fairer comparison would be based on a similar earlier period, but the best available option starts from 1958,) as observation in the Southern Hemisphere were sparse before themreferences for comparisons. Note that the difference can be partly attributed to the larger data coverage after 1979 in ERA5.

Table 1. EERIE simulations analyzed in the current study.

Institution	Alfred Wegener Institute (AWI)	Max Planck Institute (MPI-M)	Met Office (MO)	European Centre for Medium-range Weather Forecasting (ECMWF)
	Coupled atmosphere-ocean models (eddy-rich)			Atmospheric model
System name	IFS-FESOM2	ICON	HadGEM3-GC5- EERIE	IFS

Model	IFS CY48R1,	ICON-A,	UM,	IFS CY48R1
components	FESOM2, FESIM2	ICON-O	NEMO4.0.4, SI3	
Atmos. grid (km)	Tco1279 (~9 km)	R2B8 (~10 km)	N640 (~20 km at 50N)	Tco1279 (~9 km) Tco399 (~28 km)* *five ensemble members
Atmos. vertical levels (model top)	137 (0.01 hPa)	90 (0.01 hPa)	85 (85 km)	137 (0.01 hPa)
Ocean grid (km)	NG5 (~13-5 km)	R2B9 (~5 km)	eORCA12 (~8 km)	-
Ocean vertical levels	70	72	75	-
Protocol	CMIP6 HighResMIP		CMIP6 DECK	HighResMIP2
Simulations (analyzed segment lengths)	1950control (65 yrs) Historical (1950–2014)	1950control (22 years) Historical (1950-2014)	piControl (30 yrs)	Historical (1980–2023)

# 2.1.2 Atmosphere-only simulations & sensitivity experiments

220

225

230

The EERIE AMIP simulations were performed for the historical period of 1980–2023 following the HighResMIP2 highresSST-present experimental design (M. J. Roberts et al., 2024b). We analyze the simulations were produced with the IFS model, tested with in two model grid sizes (~28 km and ~9 km; both with convection parameterization), and the higher-resolution configuration is identical to the atmosphere component of the coupled IFS-FESOM2 (Table 1). One member has been performed at the 9-km resolution, but the 28-km simulations are supplemented with five ensemble members to represent a range of model uncertainty or noise. These ensembles are generated by perturbing the atmospheric initial conditions for January 1, 1980, using the same methodology employed in operational ECMWF ensemble forecasts (C. Roberts et al., 2024a).

The prescribed boundary conditions include are taken from the daily-mean SST reanalysis from the European Space Agency Sea Surface Temperature Climate Change Initiative (ESA CCI SST v3) and the daily-mean sea-ice concentration from the European Organisation for the Exploitation of Meteorological Satellites (EUMETSAT) Ocean and Sea Ice Satellite Application Facility (OSI-SAF), both retrieved on

a 0.05° ×0.05° grid. External radiative forcings are generally specified following CMIP6/HighResMIP protocols, and the specificity can be found in C. Roberts et al. (2024a).

Taking the IFS AMIP simulations as the reference (ObsSST), a series of idealized experiments with the SST boundary condition modified are carried out as part of the EERIE project. To enable exploration of the response of the atmosphere to the extratropical SST ocean mesoscale features—(C. Roberts et al., 2024b). Two types of modifications are designed. One is, EERIE project also conducted idealized experiments with modified SST boundary conditions. Taking the NoFronts experiment, in which IFS—AMIP simulations as the quasi stationary features in the extratropics are smoothed out by applying a spatial low pass filter to the climatological mean field of SST. The other is the control experiments (denoted as ObsSST), NoEddies experiment, with experiments have the transient oceanic eddy features removed from their SST boundary conditions with the same a spatial low-pass filter but applied to the SST anomaly field (difference from the climatological mean). Sea ice cover remains unchanged in all experiments. NoEddies. We emphasize that such a design of NoEddies or NoFronts experiments only allows us to test the direct thermodynamic impact from ocean mesoscales (as reflected in SSTs) but not their relative winds-currents effects (wind stress feedback; or called current feedback).

The filter being employed filter is a Gaussian filter from the GCM-Filters Python package (Loose et al., 2022). The filter length scale is set to be  $20L_R$  with a lower and higher limit of 30 km and 700 km, respectively, where  $L_R$  is the spatially varying climatological Rossby radius in the ocean- with a lower and higher limit of 30 km and 700 km, respectively. While-a filter depending on a smaller  $L_R$  at high latitudes can effectively remove the smaller oceanic eddies there, it also removes the larger-scale tropical instability waves near the equator as  $L_R$  reaches maximum. The latter consequence may obscure the interpretation on the impact of the targeted extratropical ocean mesoscales due to the tropical-extratropical teleconnections. To avoid this, low-latitude areas are masked out from the filtering with thea function with values ranging from 0 to 1:  $M(\lambda) = \frac{1}{2} \left( \tanh \left( \frac{|h-\lambda|}{s} \right) + 1 \right)$ , where h=10 determines the latitude where the M value is halved (0.5) and s=3 scales the steepness of the masking function. Like the reference simulations ObsSSST, the NoEddies experiment is run with two model grid sizes of ~28 km (five ensemble

members) and ~9 km (one member), and the NoFronts setup is only performed for the 28 km ensemble.). For more details of the experimental design, we refer readers to (C. Roberts et al., (2024b).

# 2.2 CMIP6 models & ERA5 reanalysis

For the diagnostics of SAM persistence and westerly jet characteristics, the CMIP6 models are used to compare with EERIE models. We utilize the analyze 31 CMIP6 historical simulations from the first ensemble member that provide outputs of daily geopotential at 500-hPa level and monthly zonal wind at 850 hPa. A total of 31 simulations are available, and only the period of 1980-2014 is extracted to ensure a uniform data length. All CMIP6 outputs are regridded to a uniform 1°×1° grid with the bilinear interpolation before performing the analysis—and only the period of 1980-2014 is extracted to ensure a uniform data length. As a proxy of observation, we use the global reanalysis dataset ERA5 (Hersbach et al., 2020) for the same variables and a total period from 1958 to 2023. The chosen period of ERA5 based analysis will be adjusted to align with the corresponding period of the target simulation for comparison to cover the earlier period included in some EERIE simulations. Among the reanalysis products that extend backwards in time beyond 1979 (ERA5, 20CRv3, JRA-55), ERA5 is found to agree best with station observations and produces good representation of SAM, both before and after the advent of satellite sounder data (Marshall et al., 2022). While we analyze ERA5 on the commonly distributed 0.25° ×0.25° grid, we have tested the impact with regridding it to the 1°×1° grid and fiound no notable changes in our results.

# 275 3 Diagnostics

260

265

270

280

For the overall assessment of model performance, the diagnostics described in subsections 3.1 and 3.2 below are applied to all available CMIP6 historical and EERIE simulations. Due to the limited accessibility of the EERIE data at the time of writing, diagnostics in subsections 3.3 and 3.4 are only performed on the EERIE atmosphere-only sensitivity experiments to provide more insights deeper investigation on the tropospheric mechanisms critical to the SAM persistence.

## 3.1 SAM persistence timescale

285

290

295

300

305

Some variations exist in the definition of the SAM across the literature (Ho et al., 2012), and its persistence estimation may be sensitive to the methods employed. While many studies adopt similar methodological concepts, the details are often not fully transparent. To ensure clarity, we provide a step-by-step explanation of our approach. Note that SAM is a rather barotropic feature, so even though some traditional definitions consider the vertical averaged field, we have chosen to follow Bracegirdle et al. (2020) using a single level for simplicity.

We define the SAM as the first empirical orthogonal function (EOF) of daily zonal-mean geopotential anomalies on the 500-hPa level for the region south of 20°S (Bracegirdle et al., 2020). The anomalies are calculated based on Gerber et al. (2010). First, a time series of 500-hPa zonally mean  $\overline{\Phi}(\lambda,t)$  is taken, where  $\lambda$  and t refer to latitude and time at daily intervals, respectively, and the bar indicates zonal average. Then, for each day, we subtract the global mean of 500-hPa geopotential from  $\overline{\Phi}(\lambda,t)$  at each latitude, and the resulting data is linearly detrended. Lastly, a slowly varying climatology  $\widetilde{\Phi}(\lambda,t)$  is subtracted to remove the seasonal cycle and the low-frequency nonlinear trends associated with known external forcings such as the ozone hole formation/recovery and global warming signal. The  $\widetilde{\Phi}(\lambda,t)$  field is derived in two steps: 1) Applying. First, a 60-day low-pass filter is applied to the detrended  $\overline{\Phi}(\lambda,t)$  along the t axis, which leaves us the to retain only seasonal-scale variations. 2) Then, for Second, the same date in a time axis (t) is reindexed into calendar day (t) and year, (t). For each calendar day (e.g., Jan 1st, Jan 2nd, etc.), a 30-year low-pass filter is applied, along the t axis to capture long-term variations. If the data spans less pan fewer than 30 years, the averaging of average across all available years for that same-calendar datey is performed, and hence  $\widetilde{\Phi}(\lambda,t)$  is used, resulting in a fixed, repeating annual cycle that repeats across years.

The resultant anomalies  $\overline{\Phi}'(\lambda,t)$  reflect the internal/natural variability. We can then obtain SAM as the first EOF of  $\overline{\Phi}'(\lambda,t)$  over 20–90°S. For the computation of EOFs,  $\overline{\Phi}'(\lambda,t)$  is weighted by  $\sqrt{\cos{(\lambda)}}$  to account for the decreasing distance between meridians toward the pole. The resultant leading EOF  $\mathbf{e}(\lambda)$  represents the spatial patterns of SAM, and its corresponding principal component time series PC(t) is referred to "SAM index", expressed in normalized form with zero mean and unit variance (Fig. 1a-b).

To quantify the <u>temporalSAM</u> persistence—of <u>SAM</u>, the decorrelation time scale is computed as the e-folding timescale of <u>based on</u> the autocorrelation function of the SAM index. Following the procedure in following Simpson et al. (2013), we first calculate the autocorrelation function as (2013a):

B10

325

$$\frac{\sum_{\substack{y=1 \text{PC}(d,y)\text{PC}(d+l,y)}}^{N-1} PC(d,y)PC(d+l,y)}{\sqrt{\sum_{y=1}^{N-1} PC(d,y)^2 \sum_{y=1}^{N-1} PC(d+l,y)^2}} \frac{\sum_{y=1}^{N-1} PC(d,y)PC(d+l,y)}{\sqrt{\sum_{y=1}^{N-1} PC(d,y)^2 \sum_{y=1}^{N-1} PC(d+l,y)^2}}.$$
(1)

where Here, the daily time series PC(t) has been converted to is reindexed as a function of calendar day of the year (d (e.g., Jan 1st to Dec 31st) and lag days (t), year y, and N is denotes the total number of years of the data. Equation (1) computes the autocorrelation of PC between a given day d and a lagged day d+l, averaged over all available years. The ACF(d, d) is then smoothed over a 181-day window along the d axis (to smoothen daily fluctuations) using a Gaussian filter with a full width at half maximum of 42 days (standard deviation of 8 days). Finally, for each d, an exponential curve is fitted to the smoothed ACF(d) up to a lag of 50 days using the least squares method. An, and the e-folding time scale (d) is then derived for a given d, representing the time at which the exponential fit of the ACF decreases to d0.

We found that the estimation of  $\tau(d)$  exhibits some sensitivity to the length of the data record. To provide a measure of sampling uncertainty in the ERA5of  $\tau$ , we perform 1,000 times of bootstrap resampling, each time redrawing all yearly PC(d, y) with replacement to form a new sample as large as the original sample size (same number of total years). N). Repeating the above ACF calculation for all bootstrap samples leads us to 1,000 values of  $\tau$  for a given day (Fig. 1c). The distribution of these values provides the), showing its possible range of the estimated  $\tau(d)$ .

Note that <u>we perform</u> the <u>above EOF</u> analysis <u>is performed</u> separately for <u>each datasetall datasets</u> to identify SAM as the leading mode within each simulation, allowing for potential differences in its spatial structure across models.

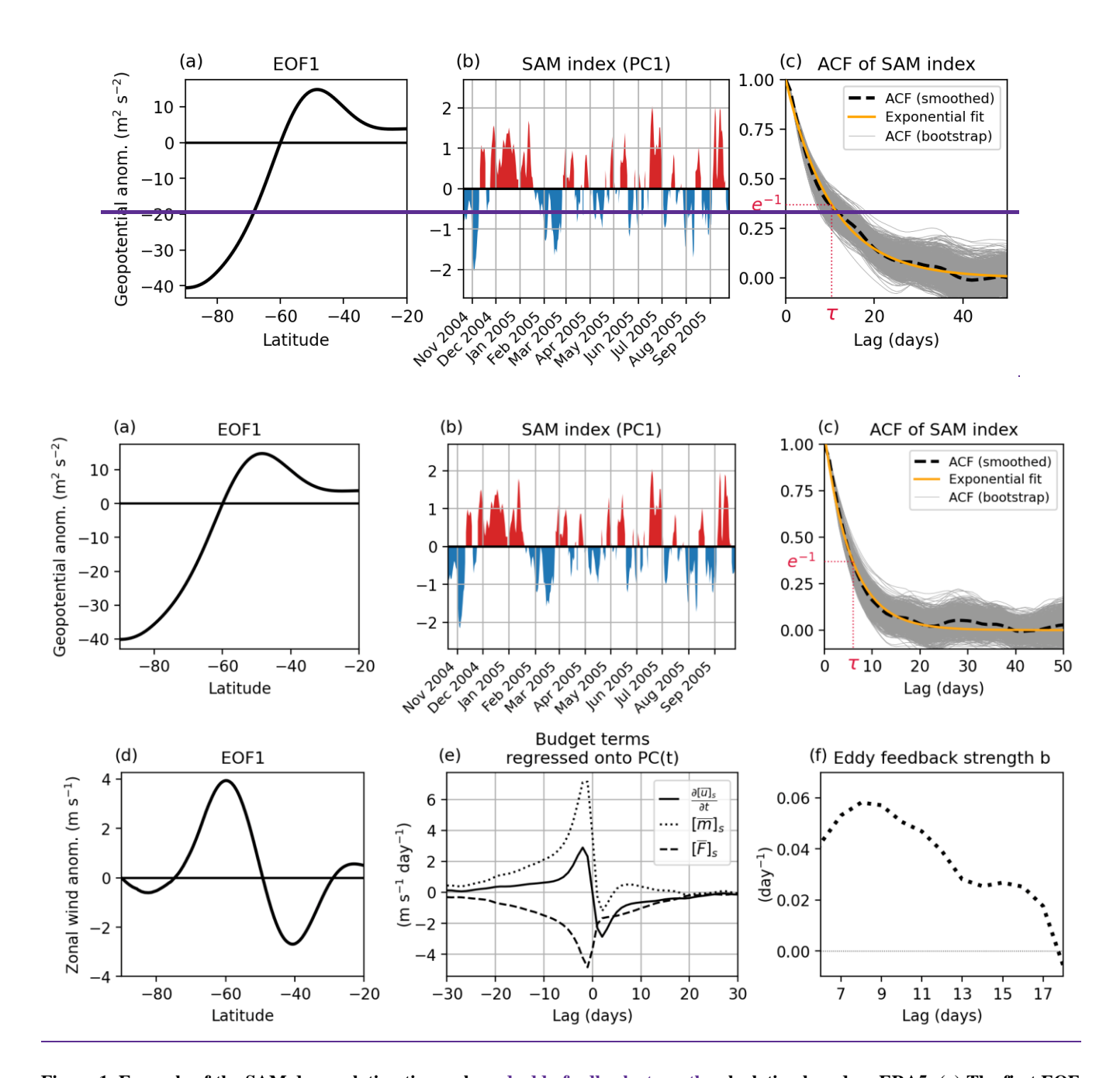


Figure 1. Example of the SAM decorrelation timescale <u>and eddy feedback strength</u> calculation based on ERA5: (a) The first EOF pattern <u>based on 500-hPa geopotential</u>; (b) <u>The</u> associated first PC1 time series (only a partial segment is shown here); (c) Autocorrelation function (ACF) of the SAM index (smoothed with a Gaussian filter) shown for a given day of the year (black dashed), and an exponential fit (yellow). The e-folding timescale is denoted as <u>Fr.</u> The <u>calculation of ACF</u> is repeated 1,000 times (gray)

with for the bootstrap sampling with replacement. samples (gray). (d) Same as (a) but based on vertically averaged zonal wind. (e) Lagged regression of the budget terms in Eqn. (3) onto the SAM index. (f) Eddy feedback strength b for lags 7–14 days.

## 3.2 Tropospheric westerly jet position

350

355

360

The westerly jet <u>position</u> is diagnosed following <u>BracegirdleMenzel</u> et al. (2020) <u>based</u>(2019) and <u>Barnes</u> and <u>Polvani</u> (2015) <u>using the output on the native model grid. We apply a quadratic fit</u> on the monthly mean zonally averaged 850-hPa zonal wind-<u>at</u> the latitude where the maximum value is found between 75°S and 10°S <u>and the four adjacent latitudes of the model</u>. The latitude where the maximum value of the <u>quadratic fit is found</u> defines the position of <u>the</u> tropospheric westerly jet, λ<sub>0</sub>.

## 345 3.3 Contribution of atmospheric eddy feedback strength to SAM persistence

In the literature. Various methods have been proposed to assess the strength of tropospheric eddy-mean flow feedback. We adopt the approach of Simpson et al. (2013b), as it has been successfully applied to potentially explainCMIP5 model evaluation and showed a high correlation with the SAM persistence bias in CMIP5 models. This approach estimates the contribution of eddy momentum flux convergence to the tendency of SAM-associated westerly wind anomalies. Therefore, within this framework, SAM is alternatively (but physics consistently) described by the first EOF of vertically averaged (pressure weighted) zonal-mean zonal wind anomalies, deseasonalized and detrended, over 20-90°S. The resultant EOF latitudinal pattern (e) and associated PC time series are defined such that the former has units of m  $s^{-1}$ <sub>7</sub> (Fig. 1d), the latter has unit variance, and their multiplication reconstructs the SAM-associated (EOF1) zonal wind anomaly fields in latitude and time space. This shift from a definition of the SAM persistence timescale using geopotential height to the zonal wind for the estimation of the eddy-mean flow feedback is based on the standard assumption that geostrophic equilibrium provides a good approximation of the relevant variables. However, ageostrophic terms can also contribute to SAM persistence, introducing limitations to this hypothesis (Vishny et al. 2024; Smith et al. 2024). For simplicity and consistency with Simpson et al. (2013b) in their CMIP5 assessment, only three pressure levels of 850, 500, 250 hPa are utilized for calculating this diagnostic analysis.

A quantity or a forcing term (denoted as X as an example) associated with the SAM is derived by projecting it onto the EOF pattern ( $\mathbf{e}$ ) with the operator:

$$[\bar{X}]_s = \frac{[\bar{\mathbf{X}}] \mathbf{W} \mathbf{e}}{\sqrt{\mathbf{e}^{\mathrm{T}} \mathbf{W} \mathbf{e}}},\tag{2}$$

where the overbars denote the zonal mean, brackets indicate the vertical average,  $[\overline{X}]$  is a vector form of  $[\overline{X}](\lambda,t)$ , where  $\lambda$  and t are latitude and time, and  $\mathbf{W}$  is a matrix with diagonal elements equal to the  $\cos(\lambda)$  weighting when defining the EOF in Simpson et al. (2013b). The resultant  $[\overline{X}]_S$  is a time series. How strongly the eddy forcing sustains the SAM wind anomalies is then estimated by projecting the vertically and zonally averaged zonal momentum tendency equation onto  $\mathbf{e}$ :

370

375

380

$$\frac{\partial [\bar{u}]_s}{\partial t} = [\bar{m}]_s + [\bar{F}]_s, \tag{3}$$

$$[\overline{m}]_s = -\left[\frac{1}{a\cos^2\lambda}\frac{\partial(\overline{u'v'}\cos^2\lambda)}{\partial\lambda}\right]_s,$$
 (4)

where  $[\overline{m}]_s$  is the eddy momentum flux convergence attributed to SAM, u' and v' are the deviation of the zonal and meridional velocities from their zonal means, respectively, and are calculated based on the instantaneous fields at 6-hourly intervals before being converted to daily means, a is the Earth radius, and  $[\overline{F}]_s$  represents all the residual momentum forcing associated with SAM. Note that Equation (3) assumes that the sum of individual projected forcing terms on the right-hand side is in balance with the tendency of the SAM anomalies. While this assumption may not be strictly mathematically-valid, Simpson et al. (2013b) demonstrated that it holds in their simulations.

Lorenz and Hartmann (2001) hypothesized that the eddy forcing of the SAM consists of a random component and a feedback component that depends linearly on the pre-existing state of SAM,  $[\overline{m}]_s = \widetilde{m} + b[\overline{u}]_s$ , where b denotes the eddy feedback strength. To obtain b, Simpson et al. (2013b) performed the lagged linear regressions of  $[\overline{m}]_s$  and  $[\overline{u}]_s$  onto the SAM index PC(t), such that for a lag day t,  $[\overline{m}]_s(t+t) \approx \beta_m(t)PC(t)$  and  $[\overline{u}]_s(t+t) \approx \beta_u(t)PC(t)$ , where  $\beta_m$  and  $\beta_u$  are the regression coefficients- $\overline{F}$  (Fig. 1e). Accordingly, the eddy forcing of SAM at lag t,  $[\overline{m}]_s(t+t)$ , can be expressed as  $\beta_m(t)PC(t) = \beta_{\widetilde{m}}(t)PC(t) + b\beta_u(t)PC(t)$ . Assuming that at sufficiently large positive lags, the feedback component dominates the eddy forcing, i.e.,  $\beta_{\widetilde{m}} \approx 0$ , we can estimate the eddy feedback strength as a function of lag days (t) by

$$b(l) = \frac{\beta_m(l)}{\beta_u(l)}.$$

In Simpson et al. (2013b), the *b* averaged over lags from 7 to 14 days is used to denote the eddy feedback strength contributing to the SAM for the intercomparison of the models- (Fig. 1f).

The approach followed here assumes that analyzing only the first PC is a good approximation to study SAM persistence. However, although the PCs are uncorrelated by construction on short timescale, this is not the case at longer lags and the coupling between the first two components influences SAM persistence (Sheshadri and Plumb 2017, Lubis and Hassanzadeh 2021, and Lubis and Hassanzadeh 2023). Analyzing only the first PC brings thus clear limitations in our analysis of the model spread in simulated SAM persistence. Furthermore, positive regression coefficients could be caused by non-stationarity of the series and in particular by interaction with the stratosphere and not just by eddy mean flow interactions. This introduces biases in the estimate of eddy feedback, particularly in late spring and summer (Byrne et al. 2016, Byrne et al. 2017), although this does not necessarily prevent using the regression method (Ma et al. 2017). The methodology is thus imperfect, but it provides an interpretative framework for the difference between the simulations and allows a comparison with earlier studies.

# 3.4 Contribution of surface wind stressfriction to SAM persistence

395

400

405

While the eddy momentum flux convergence primarily contributes positively to the persistence of SAM, it is counteracted by the negative impacts, predominantly driven-by the surface friction—(appears as a subcomponent of  $[\bar{F}]_s$  in Equation (3)), which acts to dissipate the SAM anomalies. Since the friction term for the zonal wind tendency is not directly forcing is not a standard output of EERIE simulations, we estimate it from the available from the phase 1 EERIE simulation outputs, we infer its impact from the surface—variable: the turbulent wind stress in the eastward direction. This variable, metss (or avg\_iews as renamed in the ECMWF encoding), represents (in units of N m<sup>-2</sup>). By assuming the turbulent wind stress is zero at the model top, we can estimate the friction as  $\frac{0-\rho_0^{-1}WS_0}{H_0}$ , where  $WS_0$  indicates the daily-mean eastward turbulent surface stress near the surface, resulting from turbulent atmospheric eddies near the surface (due to the roughness of the surface) and turbulent orographic form drag, represented in units of N m<sup>-2</sup>. Positive. For simplicity, we assume fixed values of metss indicate that the air flowing

over the surface exerts stress directed toward the East, which translates into a westward frictional force acting on the wind, slowing down the eastward wind tendencies.

density  $\rho_0 = 1.204 \text{ kg/m}^3$  and the atmosphere column depth  $H_0 = 8,464$  meters here. Following a similar approach for calculating  $[\overline{m}]_{\overline{s}}$ , we multiplied *metss* by -1 and  $[\overline{m}]_{\overline{s}}$ , we projected itthe result onto the EOF pattern (e) as in Equation (2) to estimate obtain the frictional forcing for the SAM zonal wind anomalies, denoted as  $[\overline{f}]_{\overline{s}}$ . Note that  $[\overline{f}]_{\overline{s}}$  does not have the same physical units as  $[\overline{m}]_{\overline{s}}$  or  $\frac{\partial [\overline{u}]_{\overline{s}}}{\partial t}$  (unit: m s<sup>-2</sup>), and thus cannot be quantitatively compared with  $[\overline{m}]_{\overline{s}}$ . Still, it is useful for the intercomparison among IFS AMIP idealized experiments to examine whether the surface friction causing the SAM dissipation mechanism is affected by the presence of ocean mesoscales features (specifically their direct thermodynamic forcing) in the SST field.  $[\overline{f}]_{s}$ . To provide an alternative measure of friction forcing and verify the estimation, the residual term of Eq. (3),  $[\overline{F}]_{s}$ , is also computed based on the estimates of the acceleration and eddy momentum flux convergence, given the dominance of friction in this residual as shown in Simpson et al. (2013b).

It is important to note that the projection values of all budget terms are resolution (number of data points)-dependent, as defined by Eq. (2). Therefore, their magnitudes are not directly comparable across datasets with differing resolutions unless regridded to a common grid, as done here.

#### 430 **4. Results**

435

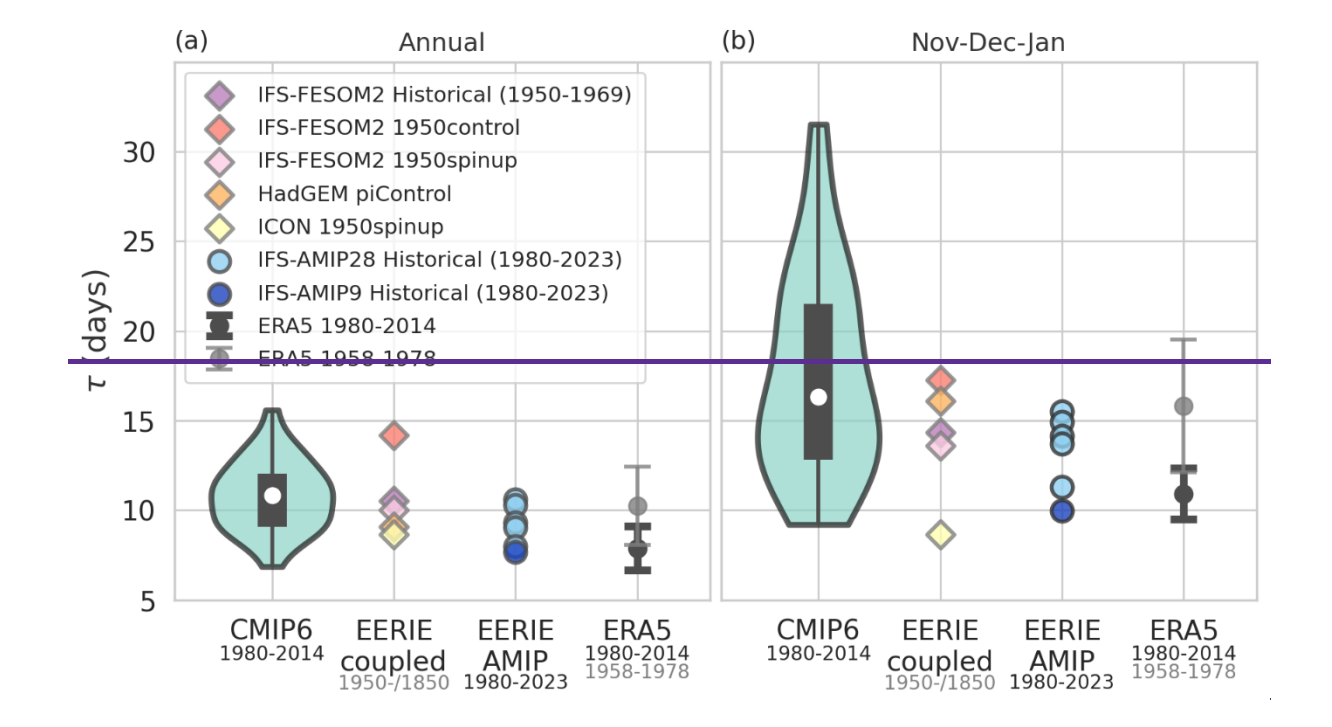
# 4.1 Model performance for SAM persistence

Figure 2 compares the performance of EERIE and CMIP6 models in representing SAM persistence, measured by the decorrelation time scale (τ). Consistent with Bracegirdle et al. (2020), CMIP6 models tend to overestimate SAM persistence compared to the reanalysis data analyzed over the same historical period (1980–2014). On the annual mean, CMIP6 presents a median value of 11 days, while the ERA5 shows a τ of 8 days. Systematically positive biases in τ seems to persist in the A reduced bias is found for EERIE coupled simulations, with a median value of 10 days. However, it should be noted that most τ of 9 days, although the distribution spread is still large, suggesting a large inter-model variability. Among these simulations, positive biases persist in the IFS-FESOM2 1950control (τ=13) and historical (τ=11)

runs, and ICON historical simulation show negative bias ( $\tau$ =6). Meanwhile, HadGEM3 *piControl* ( $\tau$ =9) 440 and ICON 1950control ( $\tau$ =8) runs are closer to ERA5. Given that some of these simulations are run under a pre-industrial 1850s' or 1950s' forcing-(even the IFS-FESOM2 historical simulation is only available for 1950-1969). The Southern Hemisphere circulation and the SAM can change over time, influenced by multiple factors such as the stratospheric ozone depletion and recovery, ENSO variability, changes in seaice extent and more. While our analysis of the SAM has removed the seasonal cycle and long-term trends, 445 some non-stationary features may remain, leading to a varying τ depending on the analysis periods. Indeed, the EERIE median value is much closer to the, we also examine the result based on an earlierperiod ERA5 (1958–1978) ERA5 result of 10.3 days,), for which τ increases to 10 days. Note, however, that there is relatively less confidence in the accuracy of the value of the SAM in ERA5 prior to the satellite era. Nevertheless, EERIE still show an improved agreement with biases that are smaller and more 450 evenly distributed on ERA5 as their τ fully cover the uncertainty ranges of ERA5 for both sides periods. During the austral early summer (NDJ), the overestimation of SAM persistence in CMIP6 is more pronounced with a longer tail of  $\tau$  distribution. The maximum and median  $\tau$  in CMIP6 is 32 days and 1617 days, respectively, compared to the ERA5 value of 11 days for the same historical period. Compared to CMIP6, EERIE coupled simulations exhibit some noticeable-improvement with the maximum and 455 median value of 17 values dropping to 20 days and 1416 days, respectively. Again, such a distribution is even less However, the spread among different EERIE simulations remains large; while the positively biased when compared to the earlier period τ are mostly captured by IFS-FESOM2, ICON tends to exhibit much smaller  $\tau$  than ERA5 ( $\tau$  of 16at 6-7 days)... 460 Interestingly, the atmosphere-only EERIE simulations (IFS-AMIP) overearly outperform the ocean-

Interestingly, the atmosphere-only EERIE simulations (IFS-AMIP) ovgenerally outperform the ocean-coupled runs—with, exhibiting a reduced positive bias in  $\tau$  compared to their coupled versions (IFS-FESOM2) and a much smaller spread—of  $\tau$ , suggesting. This suggests that the prescribed historical SST boundary condition serves a goodstrong physical constraint on the SAM persistence. With all five members considered, the simulated  $\tau$  at 28 km is still positively biased for both annual and austral-summer means, but the biases do not exceed more than 4.5 days and at least one member presents almost identical values (8 days annually and 11 days in NDJ) to ERA5- (1980-2014). Refining the atmospheric resolution from 28 km to 9 km lowers suggests a lowering of the SAM decorrelation timescale—to become slightly

negatively biased (, with  $\tau$  of 8 days annually and 10 days in NDJ) although they are still within the measurement uncertainty ranges of ERA5.



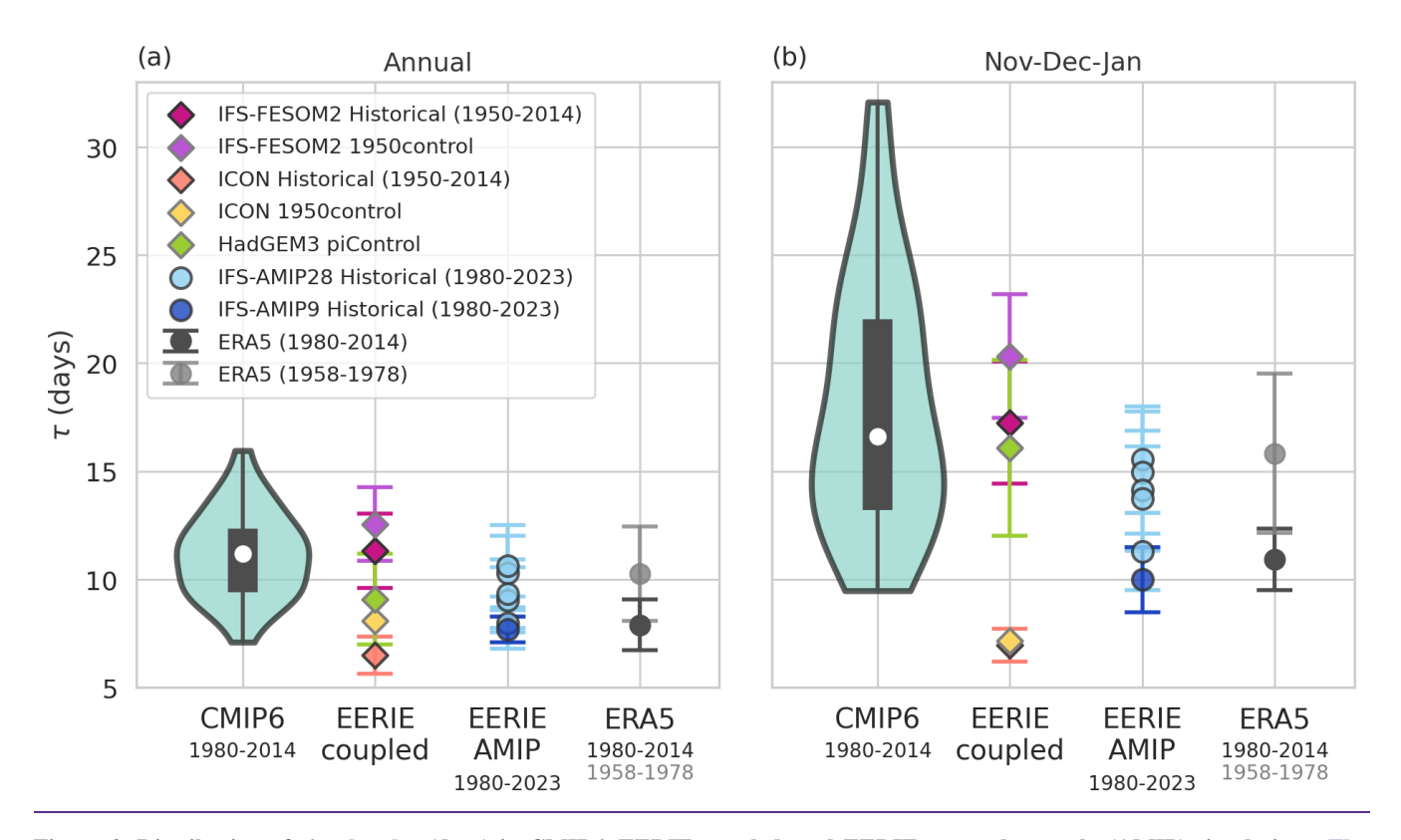


Figure 2. Distribution of simulated- $\tau$  (days) in CMIP6, EERIE coupled, and EERIE atmosphere-only (AMIP) simulations. The simulations from-CMIP6 and EERIE AMIP are both historical simulations, with theira fixed period indicated in the x-axis labels, and the simulations from-EERIE coupled vary as simulations cover varied periods as indicated in Table 1. ERA5 is analyzed for two time periods as references for. CMIP6 results from 31 experiments are presented in violin plot, in which the historical width indicates the density of the data points, the thin gray vertical box in the middle shows the 25th -75th quantiles, and pre-industrial periods, both expressed in the white dot presents the median. For the rest, error bars showingare added wherever applicable to show the  $\pm 1$  standard deviation of the results  $\pm 1$  from the 1,000 bootstrap resamplesing.

# 4.2 The relationship between jet location and $\tau$

475

480

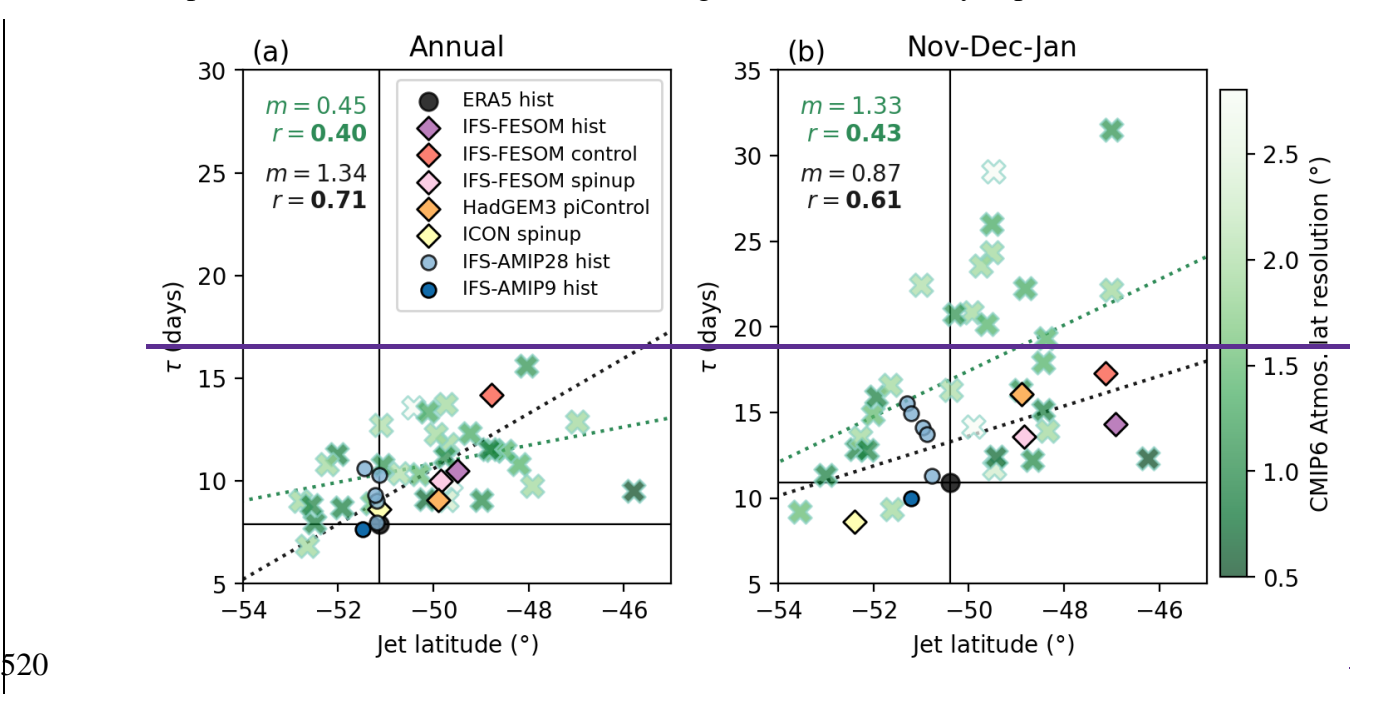
485

The bias relationship between westerly jet location ( $\lambda_0$ ) and SAM decorrelation timescale ( $\tau$ ) is then revisited. Similar to their predecessors, CMIP6 models show a positive correlation between  $\lambda_0$  and  $\tau$ , that is, models with a more equatorward jet location tend to exhibit a more persistent SAM. Consistent with Simpson & Polvani's (2016) result based on CMIP5 models, the slope of the linear fit is larger during NDJ, indicating a larger variation in  $\tau$  given the same variation in  $\lambda_0$  during this season. Examining the

model resolution of each CMIP6 simulation, there appears no strong or clear relationship between the model resolution and the model biases in these two quantities (same for both latitudinal and longitudinal resolutions and for both atmosphere and ocean models, although only the atmospheric latitudinal resolution is expressed in Fig. 3). A potential dependency on resolution could be obscured in the CMIP6 ensemble by other cancelling factors, which vary from simulations incorporating different configurations and model systems. However, it is also possible that the <u>importance of resolution (or the improvements typically</u> attributed to a-higher resolution) in determining on the performance of the-large-scale SAM variability and the mean jet hasve reached a plateau withat the typical grid size reachedsizes used in the current GCMs (e.g., CMIP6) and other factors are becoming more critical.). For instance, based on simplified atmospheric GCMs with idealized forcing, Gerber et al. (2008) found that the decorrelation timescale of the annular mode is unrealistically large at a coarse resolution of T21 (5.6°). While such a bias was notably reduced by refining the model resolution to T42 (2.8°), no further improvement was shown with a modelhigher resolution higher than T42of T85 (1.4°) and the τ converges to a still positively biased value. No test was performed in this study to determine if τ is improved again at even higher resolution or if the plateau continues.

On the annual mean, EERIE simulations generally fall within a region smaller than that covered by CMIP6, with the IFS-FESOM 1950control being the worst performing experiment among the EERIE simulations (Fig. 3a), showing both the greatest positive bias in  $\tau$  and  $\lambda_0$ . For NDJ, a clear improvement of EERIE models in representing the SAM persistence is again shown as the spread of EERIE clearly shifts toward a lower  $\tau$ , closer to ERA5's  $\tau$  compared to other CMIP6 exhibiting a similar jet location. In all, a positive  $\lambda_0$ - $\tau$  relationship remains and appears stronger in summertime across EERIE models (Fig. 3). However, the slope of the linear fit is greater for annual means than for early summer, mainly because of the specific behavior of the IFS-FESOM control. The most skillful EERIE simulations for the SAM persistence, IFS-AMIP, all well capture the jet location (with a bias < 1°). This highlights again the importance of well-represented sea surface features to the large-scale atmospheric circulation and variability. Still, even with the same IFS model and the same 28-km grid size, the five IFS-AMIP ensemble members generated by perturbing the initial conditions (the only difference is the internal atmospheric variability) exhibits a spread in  $\tau$  of about 5 days, which is not positively correlated with the

corresponding simulated jet location. This result suggests that the documented bias relationship between  $\tau$  and  $\lambda_0$  in the literature does not always hold, particularly in our IFS-AMIP setupthis configuration with prescribed SSTs. It is also possible that when the jet location is relatively has already been well-captured, other factors become increasingly important to influence the persistence of SAM, and we explore some of these potential factors in the next section using idealized sensitivity experiments.



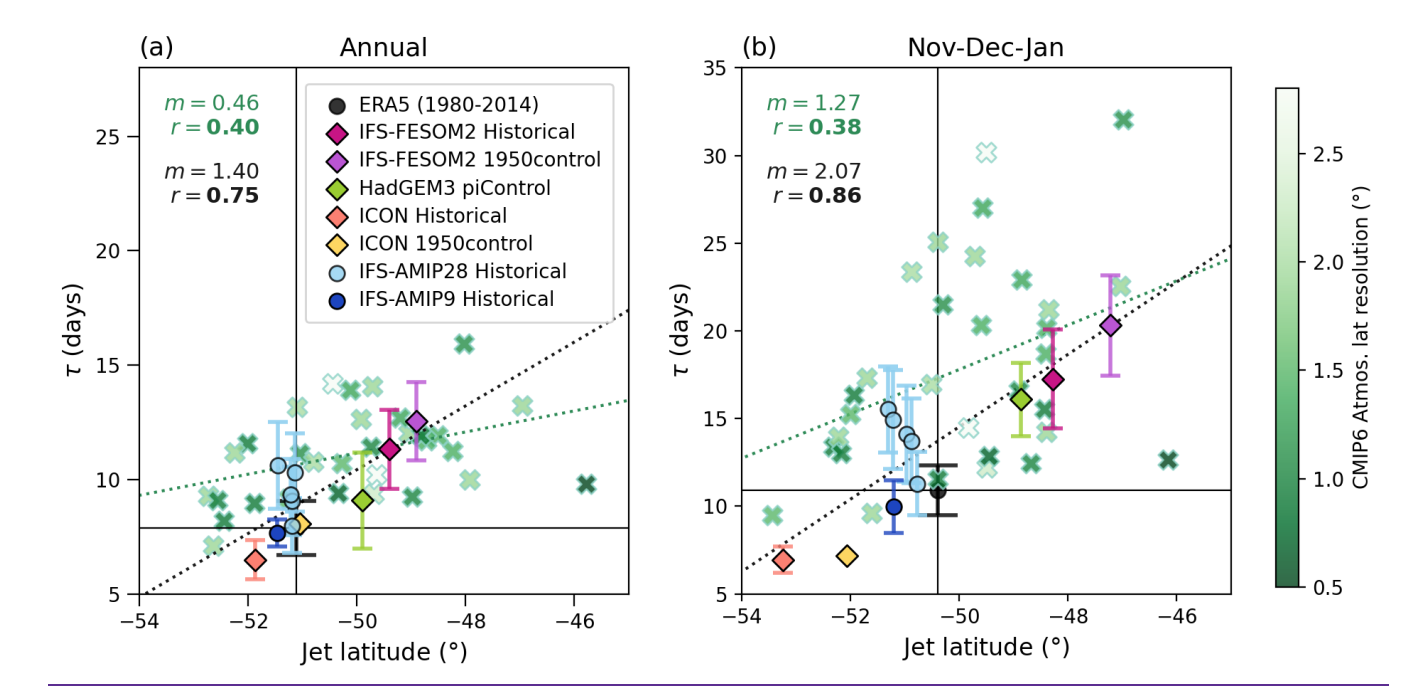


Figure 3. Scatter plot of climatological jet latitude ( $^{\circ}$ ) versus SAM decorrelation timescale  $\tau$  (days; error bar indicates  $\pm 1$  standard deviation from the bootstrapping) for (a) annual and (b) early-summer (NDJ) means in the Southern Hemisphere. Green crosses are based on CMIP6 historical simulations (colored by their latitudinal atmospheric resolution). Model names are not labeled here for visual clarity, but details are provided in their atmospheric model). Supplementary Table 1. ERA5 reanalysis and EERIE simulations are indicated as in the legend. Vertical and horizontal black lines are the ERA5 values. The green dotted straight line is the linear least-squares regression fit for CMIP6 models (slope is denoted as m, and Pearson correlation coefficient r is expressed in bold if statistically significant with the p value <0.05 in green in the top left corner). Similarly, the black dotted fitted line is the linear fit for all EERIE simulations.

# 4.3 Sensitivities to varying SST boundary conditions

525

530

535

EERIE simulations demonstrate a reduced bias in summer timesummertime SAM persistence compared to CMIP6, but identifying the cause is challenging due to variability in model systems. Although CMIP6 results show no clear link between model resolution and performance in  $\tau$  and  $\lambda_0$ , the higher resolution in EERIE remains one possible contributing factor to such an improvement. One piece of evidence is the reduction in  $\tau$  when transitioning from a 28-km to a 9-km model grid size using a consistent IFS model. Another possibility is that the new generation of models in EERIE improves model physics, reducing the biases in processes that resulted in a too overly-persistent SAM in earlier CMIP-like GCMs. In addition,

EERIE begins to explicitly resolve the ocean mesoscales, which are parameterized in CMIP6, though the resulting impacts on SAM persistence have not been investigated. To explore these possibilities, this section focuses on EERIE atmosphere-only sensitivity experiments with varied SST boundary conditions, aiming to investigate the influence of ocean mesoscales and model resolution in the observed improvement within a controlled framework.

540

560

565

We first focus on the 28-km simulations. Regarding the seasonal variation of τ (Fig. 4a), the NoEddies experiments in which ocean mesoscales are removed (either NoEddies or NoFronts) exhibit intermingled patterns overlapping with those of ObsSST. However, Although their ensemble means suggest a slight reduction in τ (by approximately 2 days) during NDJ. This result indicates that the presence in the absence of ocean eddies —hinting that mesoscale SST features, whether quasi-stationary or transient, helps may help sustain SAM persistence—this difference is not statistically significant at 95% confidence level. For the larger9-km configuration, the subtle impact of ocean eddies is not observed as NoEddies shows no clear changes in τ in the ensemble mean of from ObsSST) during this period., and both show smaller τ than the 28-km counterparts (Fig. 4b).

All these  $28 \text{ km}_{\underline{\underline{sensitivity}}}$  experiments show a slightly poleward biased jet latitude compared to ERA5 (within 1°) during NDJ, and the ensemble mean of ObsSST is the leastare generally less biased compared to those of than NoEddies and NoFronts (Fig. 4b4c). While this seems to be in agreement with the literature that a more southward-shifted jet is associated with a longer SAM persistence, there is an overall small and even negative the correlation between the  $\lambda_0$  and  $\tau$  is weak (with a correlation coefficient of 0.22 considering 03) across all IFS AMIP-simulations in the IFS-AMIP configurations.

In contrast, Compared to  $\lambda_0$ , the metric eddy feedback strength b appears a better indicator for shows a much stronger correlation with SAM persistence, exhibiting a correlation coefficient with  $\tau$  of 0.47, with a higher correlation coefficient of 0.52 and a lower p-value of 0.08 (Fig. 4c). While the p-value does not meet the conventional threshold for statistical significance (p<0.05), it is notably lower than the examined  $\lambda_0$ - $\tau$  relationship (p-value 0.42). However, the difference of b among different sets of SST-boundary-condition experiments cannot explain solely the observed reduction 4d), suggesting it may be a more informative indicator of SAM persistence in both NoEddies and NoFronts. Specifically, while the ensemble mean of NoEddies shows a slightly weaker b than this configuration. Meanwhile, the surface

friction and  $\tau$  exhibit a negative correlation (Fig. 4e) with a moderate correlation coefficient of -0.48 and p-value of 0.11. It is worth noting that of ObsSST, NoFrontsour results using  $[\bar{f}]_s$  based on surface wind stress show values similar with or even larger than ObsSST.

We then examine the surface frictional effects on SAM in these qualitatively consistent patterns with those using the residual estimates,  $[\bar{F}]_s$ , across simulations (Fig. 4d), and no clear difference in  $[\bar{f}]_s$  is found among ObsSST, NoEddies, and NoFronts. Experiments ObsSST and NoFronts exhibit highly similar values, while NoEddies exhibit a large ensemble spread and a slightly larger ensemble mean value. despite some differences in the absolute values (Fig. S1a, b). A closer examination shows that the member in NoEddies—with the largest value in  $[\bar{f}]_s$  is accompanied by the weakest eddy feedback b (red cross markers in Fig. 4e-d4d, e) and vice versa (red square markers). The opposite shifts of these two dominant mechanisms indicates an offset between each other, which explains why these members with the largest magnitudes of  $[\bar{f}]_s$  do not appear as outliers in the distribution of SAM persistence. However, the quantification of the net effects of eddy forcing and surface friction requires a comprehensive budget analysis leading to subtle combined effects on the SAM persistence.

580

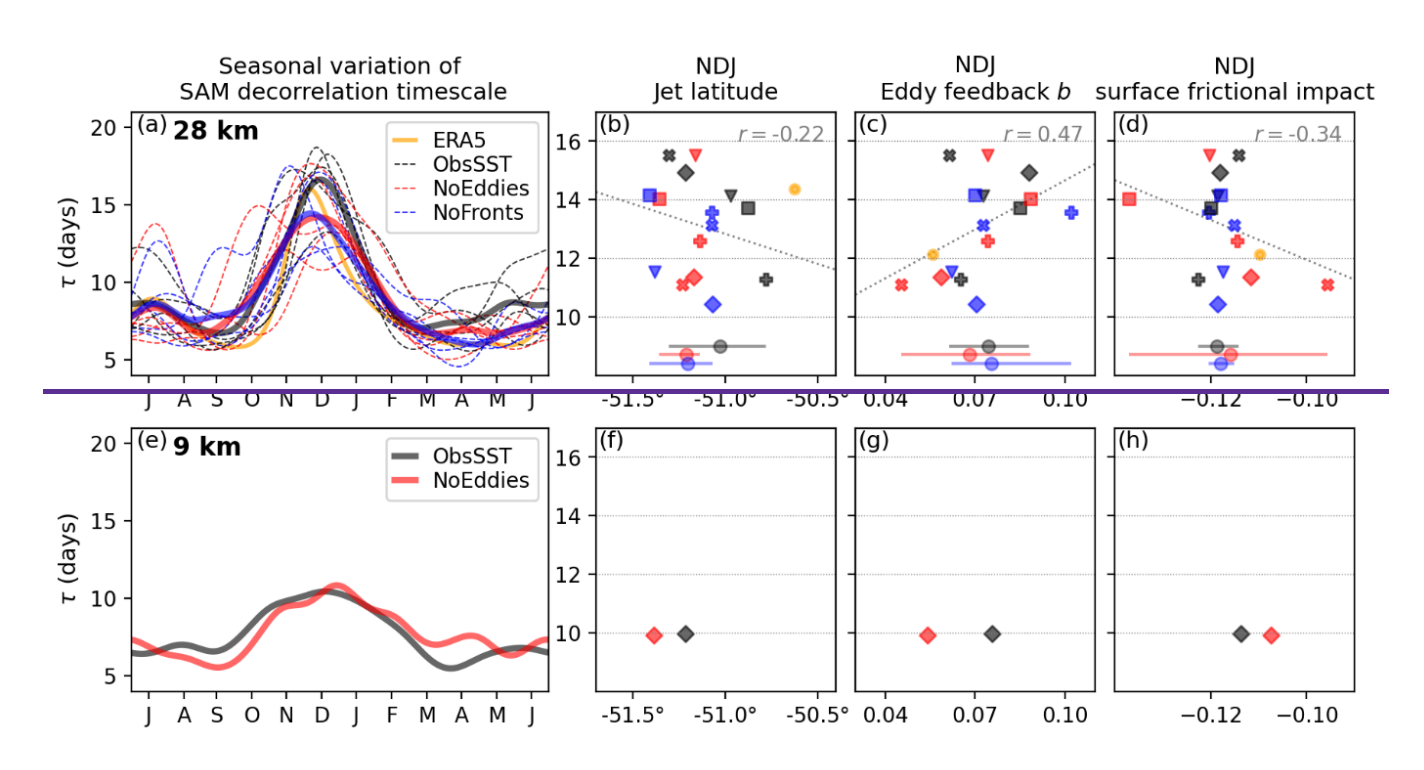
585

590

The potential impact from ocean mesoscale on the SAM persistence is, however, not observed in the 9 km simulations, as NoEddies shows almost no change from ObsSST in  $\tau$  (Fig. 4e). That said, one ensemble member may be not enough to identify the influence of the ocean eddies as the  $\tau$  fluctuation is quite large among the 28 km ensemble members, even given the same SST boundary condition. For the other metrics, the single runs of 9 km qualitatively align with the ensemble means of 28 km simulations: The suppression/filtering of ocean eddies in SST boundaries leads to a slight poleward shift (more biased than ObsSST) of the mean state jet, a weaker Lorenz and Hartmann (2001) proposed that the eddy feedback sustaining the SAM anomalies, and a slightly reduced surface can interact with the frictional impact dissipating SAM. The same signs of changes in the latter two counteracting mechanisms render their net impact on sustaining SAM uncertain. It is possible that the changes in these two processes, influenced to lengthen the effective timescale of SAM by the presence of ocean eddies, counterbalance each other at 9 km, resulting in a comparable  $\tau \frac{t_f}{(1-bt_f)}$ , where  $t_f$  is the damping timescale. Here, we estimate  $t_f$  by taking the ratio between NoEddiesthe regressed  $[\bar{u}]_S$  (in unit of m/s) and ObsSST—the

regressed  $[\bar{F}]_s$  (unit of m/s²) averaged over the 7-14 lag days, which gives a value of 8.6 days for ERA5 (close to the 8.9 days in Lorenz and Hartmann (2001)). We found that this metric indeed correlates with  $\tau$  more strongly than b or  $[\bar{f}]_s([\bar{F}]_s)$  alone with a higher correlation coefficient of 0.61 and a lower p-value of 0.03 (Fig. S1d), pointing to its superior usefulness to assess the joint impact of the two competing dominant mechanisms.

However, these analyses do notalthough those metrics explain some of the differences between individual experiments, none of them shows systematic differences between ObsSST and NoEddies and none clearly accounts for the significant reduction in  $\tau$  when the model grid size is refined from 28 km to 9 km, as all three diagnostics indicate that the 9-km simulation falls within the range of values covered by the 28-km simulations. Considering the large variability in the 28-km ensemble members, one member at 9 km may be not enough to identify the influence of the resolution. Additional simulations and diagnostics would different experimental approaches may be required to confirm the underlying cause for the observed model grid spacing dependency.



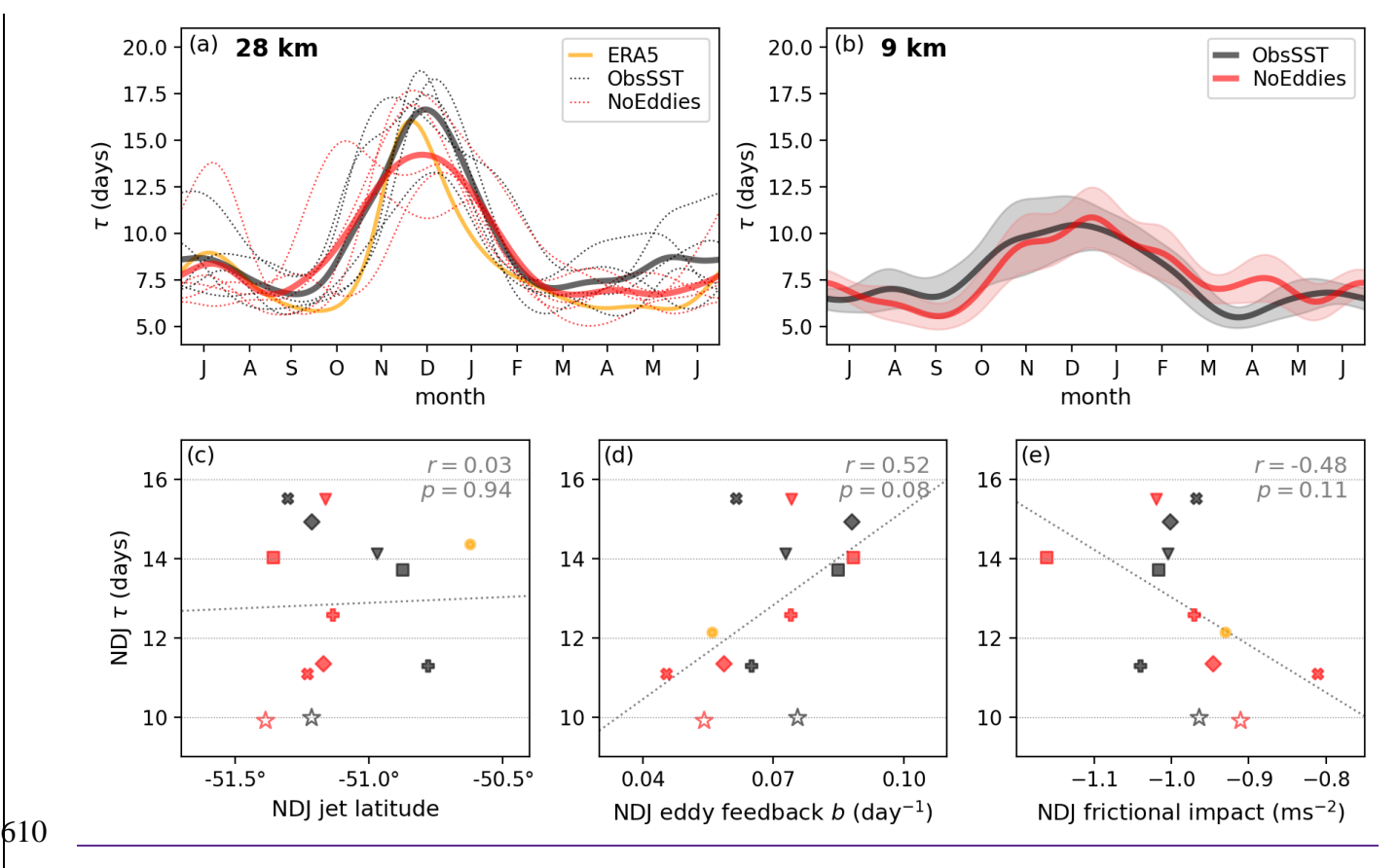


Figure 4. (a) SAM decorrelation timescale ( $\tau$ ) as a function of month for IFS-AMIP 28km simulations (dashed lines for each ensemble members and solid lines for the ensemble means; black for ObsSST and red for NoEddies experiments indicated in the legend) and ERA5 (yellow). (b(b) Similar to (a) but for 9 km experiments (shades for the  $\pm 1$  standard deviation of  $\tau$  from the 1,000 bootstrap resampling). (c) Scatter plot of  $\tau$  (days; v-axis) and westerly jet latitude (each markerx-axis; filled-color markers for one simulation; the horizontal bar in the bottom shows the minimum—to maximum—range with the circle 28 km; hollow stars for the ensemble mean of each set of the SST experiments). (c)—(9 km simulations). (d)—(e) Similar to (bc) but forwith x-axis variable replaced with the eddy feedback strength and frictional effects associated with SAMimpact, respectively. In (b)—(d), the gray dotted line represents the linear regression fit, and the correlation coefficient is and p-value are indicated in the top-right corner. (e)—(h) Same as (a)—(d), but for the 9 km simulations.

#### 620 5 Discussion and conclusions

615

This study assesses the performance of new high-resolution global model simulations developed under the EERIE project in capturing the persistence of the Southern Annular Mode (SAM), a key driver leading mode of climate variability in the Southern Hemisphere. EERIE simulations are conducted with a model

grid size of 9–28 km for the atmosphere and 5–13 km for the ocean. The persistence of the SAM is assessed using the decorrelation timescale of the SAM index  $(\tau)$ , for which CMIP GCMs have historically exhibited a systematic positive bias (overly persistent) in austral summer, often correlated with a climatological westerly jet that is too equatorward. Our conclusions and discussion based on the phase 1 preliminary simulations of the EERIE models are organized into two subsections: (1) the performance of coupled simulations, and (2) the performance of atmosphere-only (AMIP) simulations and insights obtained from the sensitivity experiments with varied SST boundary conditions under the AMIP setup.

# **5.1 EERIE Coupled simulations**

625

630

640

650

Compared to CMIP6, the EERIE coupled simulations show a slight-improvement in representing the SAM persistence on an. Although the inter-model variability remains large, the annual mean basis and a notable advancement in early summer (NDJ). The annual mean τ distribution in theof EERIE coupled simulations (clearly shifts to lower biases with a median: 10 value of 9 days) is similar to that in the CMIP6 historical simulations (median: 11 days), both are positively biased compared, closer to the ERA5 value of 8 days for 1980–2014. Notably, the EERIE simulations primarily represent than the earlier 1850s or 1950s period, for which reanalysis suggest a higher τCMIP6's median of 1011 days. For During early summer (NDJ), the EERIE simulations demonstrate τ values pronounced long tail of τ in CMIP6 simulations is also noticeably reduced in EERIEs, with the former ranging from 9 to 32 days (median: 16 days) and the latter ranging from 9 to 17 days (median: 14 days), in contrast to CMIP6's overestimated range of 9) closer to 32 days (median: 16 days). This clear improvement of the EERIE simulations for early summer τ holds regardless of the two reference periods used for ERA5 (ERA5's 11 days for the historical period as in CMIP6 and 16 days for an earlier period of 1958-1978).

. The relationship between biases in the westerly jet location ( $\lambda_0$ ) and  $\tau$  remains positively correlated in EERIE simulations as has been founddocumented for CMIP-like models. Consistently, the smaller bias for  $\tau$  in EERIE simulations during the austral summer—is accompanied by a smaller range improved representation of  $\lambda_0$  (closer to ERA5) compared to CMIP6. However, the outperformance for  $\tau$  in EERIE models compared to the CMIP6 runs that capture similar jet locations indicates that other factors in are at play. Among While the improvement of EERIE models compared to CMIP6, indicates that increased

resolution can offer benefits, the varied skills within CMIP6 in representing either  $\lambda_0$  or  $\tau$  do not show a clear dependency on the model resolution shows weak dependency on biases in either  $\lambda_0$  or  $\tau$ , but. It is possible that the impact of resolution is outweighed by other factors varying in CMIP6 simulations incorporating different configurations and model systems, or that the benefit requires the resolution exceeding a certain threshold to emerge.

## 5.2 EERIE Atmosphere-only simulations

655

660

665

670

675

Among EERIE simulations, the IFS-AMIP runs with prescribed historical SST and sea ice boundary conditions show the optimal performance in both SAM persistence and westerly jet location, with smaller spreads and closer values to ERA5 than the coupled runs. This highlights the importance of accurately representing sea surface thermal conditions to improve the simulation of these large-scale atmospheric quantities. While some studies have demonstrated Sen Gupta and England (2006) showed that the air-sea coupling is critical infor modulating the SAM (although they focused albeit focusing on interseasonal scales, timescales, which are longer than the intraseasonal scale being investigated here; Sen Gupta and England, 2006), our results suggest that the atmosphere-ocean coupling plays a secondary role relative to the. Instead, SST biases introduced by the coupling, an ongoing challenge common to ocean atmosphere in coupled GCMs (Zhang et al., 2023). Notably, the IFS AMIP historical simulations significantly reduce biases compared to CMIP6, with errors of less than 4.5 days in  $\tau$  and 1° in  $\lambda_0$  with respect to ERA5.)—appear to be more influential.

For the AMIP historical simulations, the  $\lambda_0$ – $\tau$  bias relationship does not apply, as the approximately 5-day ensemble spread in  $\tau$  shows no positive correlation with the minimally varying  $\lambda_0$ . It is possible is virtually absent. We speculate that when the jet location is already well-captured (all AMIP runs are with <1° bias) and SSTs are prescribed, other factors become increasingly important for second-order processes may come into play to affect  $\tau$ . Indeed, we find that the metrics of atmospheric eddy-mean feedback strength, surface friction and their combination correlate more strongly with  $\tau$  than with  $\lambda_0$  in the AMIP configurations, highlighting the importance of these two competing dominant mechanisms on SAM persistence of SAM. Especially, However, these metrics cannot fully explain the impact of clear reduction of  $\tau$  when the model resolution stands out and can be more clearly interpreted using the same

model. Refining the IFS model grid size is refined from 28 km to 9 km lowers the simulated  $\tau$  to even lower than the ERA5 value, although it is worth noting that ERA5 has a resolution closer to 28 km using the same atmospheric model.

680

685

690

695

700

705

The potential importance of Finally, the thermodynamic impact from the ocean mesoscale features is explored via idealized AMIP experiments. Taking the historical runs as reference (ObsSST experiment). two experiments are carried out by filtering out the quasi-stationary ocean fronts (NoFronts experiment) or the transient ocean eddies (NoEddies) in the SST boundary conditions. While three experiments (each with five ensemble members) at 28 km show intertangled seasonal variations of τ, their the difference between the 28-km ensemble means suggest of ObsSST and NoEddies imply that the presence of ocean mesoscales, regardless of fronts or eddies, mesoscale SST features may help to maintain the SAM anomalies increasing the persistence (increase  $\tau$  by roughly 2 days) in early summer. However, such an effect impact is not statistically significant and is not captured in the 9-km simulations, although there is only one ensemble member for each experiment. Among the 28-km members, we also do not see a systematic change of eddy feedback or surface friction due to the presence or absence of ocean eddies in the SST field. The critical role of oceanic mesoscale eddies in the Southern Ocean climate system is well documented. While their local impact on the atmospheric boundary layer is well established, their direct influence in modulating large-scale modes such as the SAM appears limited under our AMIP setup without air-sea coupling. A similar conclusion was obtained by Purich et al. (2021) performed similar experiments but with a coarser coupled GCM, (model resolution of ~130 km), ACCESS1.0, to explore the role of oceanic variability on SAM by restoring the SST to the monthly mean patterns. They found that suppressing Southern Ocean SST variability by restoring the SST to the monthly mean patterns does not impact SAM persistence in their simulations, but their analysis was on monthly rather than daily means and with a coarser model resolution of ~130 km. As they also concluded, that eddy-resolving models are required to properly capture the air—sea feedbacks in the Southern Hemisphere.

Using the idealized AMIP experiments, we conduct further exploration on the "internal" atmospheric dynamical mechanisms contributing to the SAM persistence, eddy feedback strength and surface friction. It is worth noting that the eddy feedback strength appears to be a better indicator than the mean state jet latitude  $\lambda_0$ , linking positively and more statistically significantly to the simulated summertime  $\tau$  among

the IFS AMIP simulations. Still, by how much it is counteracted by the surface friction requires a more comprehensive budget analysis. Likely because of those compensating effects, the metrics of jet latitude, eddy feedback and frictional impact, do not provide a clear answer as to what contribute to the observed differences in the simulated  $\tau$  when ocean mesoscales are removed.

710

715

720

730

This result highlights the complexity of mechanisms contributing to the SAM persistence in GCMs. For instance, the interplay between eddy forcing and surface friction suggests that even small errors in one process may result in notable uncertainty in their net impact. Additionally Between EERIE coupled and AMIP simulations, the superior performance of the latter seems to suggest that model skills in representing SAM persistence does not clearly benefit from the two-way ocean-atmosphere coupling or from the explicit inclusion of ocean mesoscale features. Our hypothesis is that while coupled models offer a more physically consistent representation of the climate system, they also tend to introduce SST biases—potentially due to under-tuning in high-resolution configurations or imbalances in the coupling process. In fact, previous studies have shown that eddy-permitting models can exhibit larger SST biases than either coarser models with parameterized eddy fluxes or fully eddy-rich models (e.g., Storkey et al. 2025). Reducing SST biases remains essential for advancing the representation of SAM and Southern Hemisphere climate variability. The large variability among ensemble members with the same model configuration also highlights the complexity of mechanisms contributing to the SAM persistence in GCMs and call for further investigation or different approaches to address the outstanding questions. For example, this study only considers the zonally averaged properties, but non-zonal components likely play important roles in shaping SAM characteristics in climate systems and hence their representation in GCMs (e.g., Barnes and Hartmann, 2010; Sen Gupta and England, 2006). Nevertheless, the general improvements seen in the phase 1 simulations of the EERIE coupled models present a-promising path forwardresults in addressing the long-standing GCM biases in SAM persistence, especially considering the challenges in optimally configuring high-resolution models (i.e., tuning) and the lack of community experience in doing so. Furthermore, the controlled framework of the IFS-AMIP idealized eddy-rich experiments offers significant potential for enhancing our understanding of atmospheric responses to ocean mesoscales.

## Acknowledgments

This publication is part of the EERIE project funded by the European Union. Views and opinions expressed are however those of the author(s) only and do not necessarily reflect those of the European Union or the European Climate Infrastructure and Environment Executive Agency (CINEA). Neither the European Union nor the granting authority can be held responsible for them. This work has received funding from the Swiss State Secretariat for Education, Research and Innovation (SERI) under contract #22.00366. This work was funded by UK Research and Innovation (UKRI) under the UK government's Horizon Europe funding guarantee (grant number 10057890, 10049639, 10040510, 10040984). Hugues Goosse is Research Director with the Fonds de la Recherche Scientifique (F.R.S. -FNRS). The authors also thank Francesco Ragone, Isla Simpson, Matthew Patterson, Thomas Bracegirdle for providing constructive suggestions or clarification about the methodologies employed in their works.

## **Data Availability Statement**

All EERIE simulation outputs are publicly accessible at <a href="https://eerie.cloud.dkrz.de">https://eerie.cloud.dkrz.de</a> and Wachsmann et al. (2024). The calculation of EOFs was performed using the publicly available Python package by Dawson (2016). All scripts used for the analysis and figure generation will be shared in the GitHub repository under the EERIE project (<a href="https://github.com/eerie-project">https://github.com/eerie-project</a>) upon acceptance of the publication.

#### References

755

- 750 Barnes, E.A., Hartmann, D.L., 2010. Dynamical Feedbacks of the Southern Annular Mode in Winter and Summer. J. Atmospheric Sci. 67, 2320–2330. <a href="https://doi.org/10.1175/2010JAS3385.1">https://doi.org/10.1175/2010JAS3385.1</a>
  - Barnes, E. A., and L. M. Polvani, 2015. CMIP5 Projections of Arctic Amplification, of the North American/North Atlantic Circulation, and of Their Relationship. J. Climate, 28, 5254–5271, https://doi.org/10.1175/JCLI-D-14-00589.1.
  - Bishop, S. P., R. J. Small, F. O. Bryan, and R. A. Tomas, 2017. Scale Dependence of Midlatitude Air—Sea Interaction. J. Climate, 30, 8207–8221, https://doi.org/10.1175/JCLI-D-17-0159.1.
  - Bracegirdle, T.J., Holmes, C.R., Hosking, J.S., Marshall, G.J., Osman, M., Patterson, M., Rackow, T., 2020. Improvements in Circumpolar Southern Hemisphere Extratropical Atmospheric Circulation in CMIP6 Compared to CMIP5. Earth Space Sci. 7, e2019EA001065. https://doi.org/10.1029/2019EA001065

- Busecke, J.J.M., Abernathey, R.P., 2019. Ocean mesoscale mixing linked to climate variability. Sci. Adv. 5, eaav5014. <a href="https://doi.org/10.1126/sciadv.aav5014">https://doi.org/10.1126/sciadv.aav5014</a>
- Byrne, N. J., Shepherd, T. G., Woollings, T., & Plumb, R. A., 2016. Annular modes and apparent eddy feedbacks in the Southern Hemisphere. Geophysical Research Letters, 43(8), 3897–3902. https://doi.org/10.1002/2016GL068851
  - Byrne, N. J., Shepherd, T. G., Woollings, T., & Plumb, R. A., 2017. Nonstationarity in Southern Hemisphere Climate Variability Associated with the Seasonal Breakdown of the Stratospheric Polar Vortex. Journal of Climate, 30(18), 7125–7139. https://doi.org/10.1175/JCLI-D-17-0097.1
- 770 Campitelli, E., Díaz, L.B., Vera, C., 2022. Assessment of zonally symmetric and asymmetric components of the Southern Annular Mode using a novel approach. Clim. Dyn. 58, 161–178. https://doi.org/10.1007/s00382-021-05896-5
  - Chassignet, E.P., Xu, X., 2021. On the Importance of High-Resolution in Large-Scale Ocean Models. Adv. Atmospheric Sci. 38, 1621–1634. https://doi.org/10.1007/s00376-021-0385-7
- 775 Codron, F., 2005. Relation between Annular Modes and the Mean State: Southern Hemisphere Summer. J. Clim. 18, 320–330. https://doi.org/10.1175/JCLI-3255.1

785

- Dawson, A., 2016. eofs: A Library for EOF Analysis of Meteorological, Oceanographic, and Climate Data. J. Open Res. Softw. 4, 14. https://doi.org/10.5334/jors.122
- Ding, Q., Steig, E.J., Battisti, D.S., Wallace, J.M., 2012. Influence of the Tropics on the Southern Annular Mode. J. Clim. 25, 6330–6348. https://doi.org/10.1175/JCLI-D-11-00523.1
- Doddridge, E.W., Marshall, J., 2017. Modulation of the Seasonal Cycle of Antarctic Sea Ice Extent Related to the Southern Annular Mode. Geophys. Res. Lett. 44, 9761–9768. https://doi.org/10.1002/2017GL074319
- European Commission, 2022. European Eddy-RIch ESMs [WWW Document]. URL https://doi.org/10.3030/101081383 (accessed 2.2.25).
- Eyring, V., Bony, S., Meehl, G.A., Senior, C.A., Stevens, B., Stouffer, R.J., Taylor, K.E., 2016. Overview of the Coupled Model Intercomparison Project Phase 6 (CMIP6) experimental design and organization. Geosci. Model Dev. 9, 1937–1958. https://doi.org/10.5194/gmd-9-1937-2016
- Fogt, R.L., Marshall, G.J., 2020. The Southern Annular Mode: Variability, trends, and climate impacts across the Southern Hemisphere. WIREs Clim. Change 11, e652. <a href="https://doi.org/10.1002/wcc.652">https://doi.org/10.1002/wcc.652</a>
- Frenger, I., Gruber, N., Knutti, R., Münnich, M., 2013. Imprint of Southern Ocean eddies on winds, clouds and rainfall. Nature Geosci 6, 608–612. https://doi.org/10.1038/ngeo1863
- Gerber, E.P., Baldwin, M.P., Akiyoshi, H., Austin, J., Bekki, S., Braesicke, P., Butchart, N., Chipperfield, M., Dameris, M., Dhomse, S., Frith, S.M., Garcia, R.R., Garny, H., Gettelman, A., Hardiman, S.C., Karpechko, A., Marchand, M., Morgenstern, O., Nielsen, J.E., Pawson, S., Peter, T., Plummer, D.A., Pyle, J.A., Rozanov, E., Scinocca, J.F., Shepherd, T.G., Smale, D., 2010. Stratosphere-troposphere coupling and annular mode variability in chemistry-climate models. J. Geophys. Res. Atmospheres 115, 2009JD013770. https://doi.org/10.1029/2009JD013770
- 800 Gerber, E.P., Voronin, S., Polvani, L.M., 2008. Testing the Annular Mode Autocorrelation Time Scale in Simple Atmospheric General Circulation Models. Mon. Weather Rev. 136, 1523–1536. https://doi.org/10.1175/2007MWR2211.1

- Gillett, N.P., Kell, T.D., Jones, P.D., 2006. Regional climate impacts of the Southern Annular Mode. Geophys. Res. Lett. 33, 2006GL027721. https://doi.org/10.1029/2006GL027721
- Haarsma, R.J., Roberts, M.J., Vidale, P.L., Senior, C.A., Bellucci, A., Bao, Q., Chang, P., Corti, S., 805 Fučkar, N.S., Guemas, V., Von Hardenberg, J., Hazeleger, W., Kodama, C., Koenigk, T., Leung, L.R., Lu, J., Luo, J.-J., Mao, J., Mizielinski, M.S., Mizuta, R., Nobre, P., Satoh, M., Scoccimarro, E., Semmler, T., Small, J., Von Storch, J.-S., 2016. High Resolution Model Intercomparison **Project** (HighResMIP v1.0)for CMIP6. Geosci. Model Dev. 9. 4185-4208. 810 https://doi.org/10.5194/gmd-9-4185-2016https://doi.org/10.5194/gmd-9-4185-2016
  - Hassanzadeh, P., and Kuang, Z., 2019. Quantifying the Annular Mode Dynamics in an Idealized Atmosphere. J. Atmos. Sci., 76, 1107–1124, https://doi.org/10.1175/JAS-D-18-0268.1.
- Hersbach, H., Bell, B., Berrisford, P., Hirahara, S., Horányi, A., Muñoz-Sabater, J., Nicolas, J., Peubey, C., Radu, R., Schepers, D., Simmons, A., Soci, C., Abdalla, S., Abellan, X., Balsamo, G.,
  Bechtold, P., Biavati, G., Bidlot, J., Bonavita, M., De Chiara, G., Dahlgren, P., Dee, D., Diamantakis, M., Dragani, R., Flemming, J., Forbes, R., Fuentes, M., Geer, A., Haimberger, L., Healy, S., Hogan, R.J., Hólm, E., Janisková, M., Keeley, S., Laloyaux, P., Lopez, P., Lupu, C., Radnoti, G., De Rosnay, P., Rozum, I., Vamborg, F., Villaume, S., Thépaut, J., 2020. The ERA5 global reanalysis. Q. J. R. Meteorol. Soc. 146, 1999–2049. https://doi.org/10.1002/qj.3803
- Hewitt, H.T., Roberts, M., Mathiot, P., Biastoch, A., Blockley, E., Chassignet, E.P., Fox-Kemper, B., Hyder, P., Marshall, D.P., Popova, E., Treguier, A.-M., Zanna, L., Yool, A., Yu, Y., Beadling, R., Bell, M., Kuhlbrodt, T., Arsouze, T., Bellucci, A., Castruccio, F., Gan, B., Putrasahan, D., Roberts, C.D., Van Roekel, L., Zhang, Q., 2020. Resolving and Parameterising the Ocean Mesoscale in Earth System Models. Curr. Clim. Change Rep. 6, 137–152. https://doi.org/10.1007/s40641-020-00164-w
  - Ho, M., Kiem, A.S., Verdon-Kidd, D.C., 2012. The Southern Annular Mode: a comparison of indices. Hydrol. Earth Syst. Sci. 16, 967–982. https://doi.org/10.5194/hess-16-967-2012
  - Karoly, D.J., 1989. Southern Hemisphere Circulation Features Associated with El Niño-Southern Oscillation Events. J. Clim. 2, 1239–1252. https://doi.org/10.1175/1520-0442(1989)002<1239:SHCFAW>2.0.CO;2
  - Kidston, J., Gerber, E.P., 2010. Intermodel variability of the poleward shift of the austral jet stream in the CMIP3 integrations linked to biases in 20th century climatology. Geophys. Res. Lett. 37, 2010GL042873. https://doi.org/10.1029/2010GL042873
- Lefebvre, W., Goosse, H., 2005. Influence of the Southern Annular Mode on the sea ice-ocean system: the role of the thermal and mechanical forcing. Ocean Sci. 1, 145–157. https://doi.org/10.5194/os-1-145-2005

- Lenton, A., Matear, R.J., 2007. Role of the Southern Annular Mode (SAM) in Southern Ocean CO<sub>2</sub> uptake. Glob. Biogeochem. Cycles 21, 2006GB002714. https://doi.org/10.1029/2006GB002714
- Lim, E.-P., Hendon, H.H., Rashid, H., 2013. Seasonal Predictability of the Southern Annular Mode due to Its Association with ENSO. J. Clim. 26, 8037–8054. https://doi.org/10.1175/JCLI-D-13-00006.1
  - Loose, N., Abernathey, R., Grooms, I., Busecke, J., Guillaumin, A., Yankovsky, E., Marques, G., Steinberg, J., Ross, A., Khatri, H., Bachman, S., Zanna, L., Martin, P., 2022. GCM-Filters: A

- Python Package for Diffusion-based Spatial Filtering of Gridded Data. J. Open Source Softw. 7, 3947. https://doi.org/10.21105/joss.03947
  - Lorenz, D.J., Hartmann, D.L., 2001. Eddy–Zonal Flow Feedback in the Southern Hemisphere. J. Atmospheric Sci. 58, 3312–3327. https://doi.org/10.1175/1520-0469(2001)058<3312:EZFFIT>2.0.CO;2
- Lovenduski, N.S., Gruber, N., 2005. Impact of the Southern Annular Mode on Southern Ocean circulation and biology. Geophys. Res. Lett. 32, 2005GL022727. <a href="https://doi.org/10.1029/2005GL022727https://doi.org/10.1029/2005GL022727">https://doi.org/10.1029/2005GL022727</a>
  - Lubis, S. W., and P. Hassanzadeh, 2021. An Eddy–Zonal Flow Feedback Model for Propagating Annular Modes. J. Atmos. Sci., 78, 249–267, https://doi.org/10.1175/JAS-D-20-0214.1.
- Lubis, S. W., & Hassanzadeh, P., 2023. The Intrinsic 150-Day Periodicity of the Southern Hemisphere

  Extratropical Large-Scale Atmospheric Circulation. AGU Advances, 4(3), e2022AV000833. 
  https://doi.org/10.1029/2022AV000833
  - Ma, D., Hassanzadeh, P., & Kuang, Z., 2017. Quantifying the Eddy–Jet Feedback Strength of the Annular Mode in an Idealized GCM and Reanalysis Data. Journal of the Atmospheric Sciences, 74(2), 393–407. https://doi.org/10.1175/JAS-D-16-0157.1
- Marshall, G. J., 2003: Trends in the Southern Annular Mode from Observations and Reanalyses. J. Climate, 16, 4134–4143, https://doi.org/10.1175/1520-0442(2003)016<4134:TITSAM>2.0.CO;2.

- Marshall, G. J., Fogt, R. L., Turner, J., & Clem, K. R., 2022. Can current reanalyses accurately portray changes in Southern Annular Mode structure prior to 1979?. Climate Dynamics, 59(11), 3717-3740, https://doi.org/10.1007/s00382-022-06292-3.
- Menzel, M. E., Waugh, D., & Grise, K., 2019. Disconnect Between Hadley Cell and Subtropical Jet Variability and Response to Increased CO2. Geophysical Research Letters, 46(12), 7045-7053. https://doi.org/10.1029/2019GL083345
- Purich, A., Boschat, G., Liguori, G., 2021. Assessing the impact of suppressing Southern Ocean SST variability in a coupled climate model. Sci. Rep. 11, 22069. https://doi.org/10.1038/s41598-021-01306-2
  - Roberts, C., Aengenheyster, M., Roberts, M., 2024a. Description of EERIE atmosphere-only reference simulations. https://doi.org/10.5281/ZENODO.14334612
  - Roberts, C., Aengenheyster, M., Roberts, M., 2024b. Description of EERIE idealised atmosphere-only simulations. https://doi.org/10.5281/ZENODO.14514510
    - Roberts, M.J., Jung, T., Ortega, P., Ghosh, R., Wachsmann, F., von Storch, J.-S., Kroeger, J., Aengenheyster, M., Roberts, C., 2024a. Phase 1 simulations, including HighResMIP and CMIP6-PI-control simulations. https://doi.org/10.5281/ZENODO.14288726
- Roberts, M.J., Reed, K.A., Bao, Q., Barsugli, J.J., Camargo, S.J., Caron, L.-P., Chang, P., Chen, C.-T., Christensen, H.M., Danabasoglu, G., Frenger, I., Fučkar, N.S., Hasson, S.U., Hewitt, H.T., Huang, H., Kim, D., Kodama, C., Lai, M., Leung, L.-Y.R., Mizuta, R., Nobre, P., Ortega, P., Paquin, D., Roberts, C.D., Scoccimarro, E., Seddon, J., Treguier, A.M., Tu, C.-Y., Ullrich, P.A., Vidale, P.L., Wehner, M.F., Zarzycki, C.M., Zhang, B., Zhang, W., Zhao, M., 2024b. High Resolution Model Intercomparison Project phase 2 (HighResMIP2) towards CMIP7. https://doi.org/10.5194/egusphere-2024-2582https://doi.org/10.5194/egusphere-2024-2582

- Robinson, W. A., 2000. A Baroclinic Mechanism for the Eddy Feedback on the Zonal Index. J. Atmos. Sci., 57, 415–422, https://doi.org/10.1175/1520-0469(2000)057<0415:ABMFTE>2.0.CO;2.
- Saggioro, E., & Shepherd, T. G., 2019. Quantifying the Timescale and Strength of Southern Hemisphere Intraseasonal Stratosphere-troposphere Coupling. Geophysical Research Letters, 46(22), 13479—13487. https://doi.org/10.1029/2019GL084763

895

905

- Sen Gupta, A., England, M.H., 2006. Coupled Ocean–Atmosphere–Ice Response to Variations in the Southern Annular Mode. J. Clim. 19, 4457–4486. <a href="https://doi.org/10.1175/JCLI3843.1">https://doi.org/10.1175/JCLI3843.1</a>
- Sheshadri, A., & Plumb, R. A., 2017. Propagating Annular Modes: Empirical Orthogonal Functions, Principal Oscillation Patterns, and Time Scales. Journal of the Atmospheric Sciences, 74(5), 1345–1361. https://doi.org/10.1175/JAS-D-16-0291.1
- Simpson, I. R., Hitchcock, P., Shepherd, T. G., & Scinocca, J. F., 2011. Stratospheric variability and tropospheric annular-mode timescales. Geophysical Research Letters, 38(20). https://doi.org/10.1029/2011GL049304
- 900 Simpson, I.R., Hitchcock, P., Shepherd, T.G., Scinocca, J.F., 2013a. Southern Annular Mode Dynamics in Observations and Models. Part I: The Influence of Climatological Zonal Wind Biases in a Comprehensive GCM. J. Clim. 26, 3953–3967. https://doi.org/10.1175/JCLI-D-12-00348.1
  - Simpson, I.R., Polvani, L.M., 2016. Revisiting the relationship between jet position, forced response, and annular mode variability in the southern midlatitudes. Geophys. Res. Lett. 43, 2896–2903. https://doi.org/10.1002/2016GL067989
  - Simpson, I.R., Shepherd, T.G., Hitchcock, P., Scinocca, J.F., 2013b. Southern Annular Mode Dynamics in Observations and Models. Part II: Eddy Feedbacks. J. Clim. 26, 5220–5241. https://doi.org/10.1175/JCLI-D-12-00495.1
  - Smith, S., Lu, J., & Staten, P. W., 2024. Diabatic Eddy Forcing Increases Persistence and Opposes Propagation of the Southern Annular Mode in MERRA-2. J. Atmos. Sci., 81, 743–764. https://doi.org/10.1175/JAS-D-23-0019.1
- Son, S. -W., Gerber, E.P., Perlwitz, J., Polvani, L.M., Gillett, N.P., Seo, K. -H., Eyring, V., Shepherd, T.G., Waugh, D., Akiyoshi, H., Austin, J., Baumgaertner, A., Bekki, S., Braesicke, P., Brühl, C., Butchart, N., Chipperfield, M.P., Cugnet, D., Dameris, M., Dhomse, S., Frith, S., Garny, H., Garcia, R., Hardiman, S.C., Jöckel, P., Lamarque, J.F., Mancini, E., Marchand, M., Michou, M., Nakamura, T., Morgenstern, O., Pitari, G., Plummer, D.A., Pyle, J., Rozanov, E., Scinocca, J.F., Shibata, K., Smale, D., Teyssèdre, H., Tian, W., Yamashita, Y., 2010. Impact of stratospheric ozone on Southern Hemisphere circulation change: A multimodel assessment. J. Geophys. Res. Atmospheres

  115,
  2010JD014271. https://doi.org/10.1029/2010JD014271https://doi.org/10.1029/2010JD014271
  - Storkey, D., Mathiot, P., Bell, M. J., Copsey, D., Guiavarc'h, C., Hewitt, H. T., Ridley, J., and Roberts, M. J., 2024. Resolution dependence of interlinked Southern Ocean biases in global coupled HadGEM3 models, EGUsphere [preprint], https://doi.org/10.5194/egusphere-2024-1414.
- Thompson, D.W.J., Solomon, S., Kushner, P.J., England, M.H., Grise, K.M., Karoly, D.J., 2011.

  Signatures of the Antarctic ozone hole in Southern Hemisphere surface climate change. Nat. Geosci. 4, 741–749. <a href="https://doi.org/10.1038/ngeo1296">https://doi.org/10.1038/ngeo1296</a>

- Vishny, D. N., Wall, C. J., & Lutsko, N. J., 2024. Impact of Atmospheric Cloud Radiative Effects on Annular Mode Persistence in Idealized Simulations. Geophysical Research Letters, 51(15), e2024GL109420. https://doi.org/10.1029/2024GL109420
- 930 Wachsmann, F., Matthias Aengenheyster, Wickramage, C., Seddon, J., Nikolay Koldunov, Ziemen, F., 2024. Data access to EERIE ESM output via intake catalogues: Phase1 plus Hackathon simulations.

940

- https://doi.org/10.5281/ZENODO.14243677https://doi.org/10.5281/ZENODO.14243677
- Xia, X., & Chang, E. K. M., 2014. Diabatic Damping of Zonal Index Variations. Journal of the Atmospheric Sciences, 71(8), 3090–3105. https://doi.org/10.1175/JAS-D-13-0292.1
- Zhang, Q., Liu, B., Li, S., Zhou, T., 2023. Understanding Models' Global Sea Surface Temperature Bias in Mean State: From CMIP5 to CMIP6. Geophys. Res. Lett. 50, e2022GL100888. https://doi.org/10.1029/2022GL100888https://doi.org/10.1029/2022GL100888
- Zhang, X., He, B., Liu, Y., Bao, Q., Zheng, F., Li, J., Hu, W., & Wu, G., 2022. Evaluation of the seasonality and spatial aspects of the Southern Annular Mode in CMIP6 models. International Journal of Climatology, 42(7), 3820-3837. https://doi.org/10.1002/joc.7447
- Zurita-Gotor, P., J. Blanco-Fuentes, and E. P. Gerber, 2014. The Impact of Baroclinic Eddy Feedback on the Persistence of Jet Variability in the Two-Layer Model. J. Atmos. Sci., 71, 410–429, https://doi.org/10.1175/JAS-D-13-0102.1